Cell Reports

Article

Diribonuclease activity eliminates toxic diribonucleotide accumulation

Graphical abstract

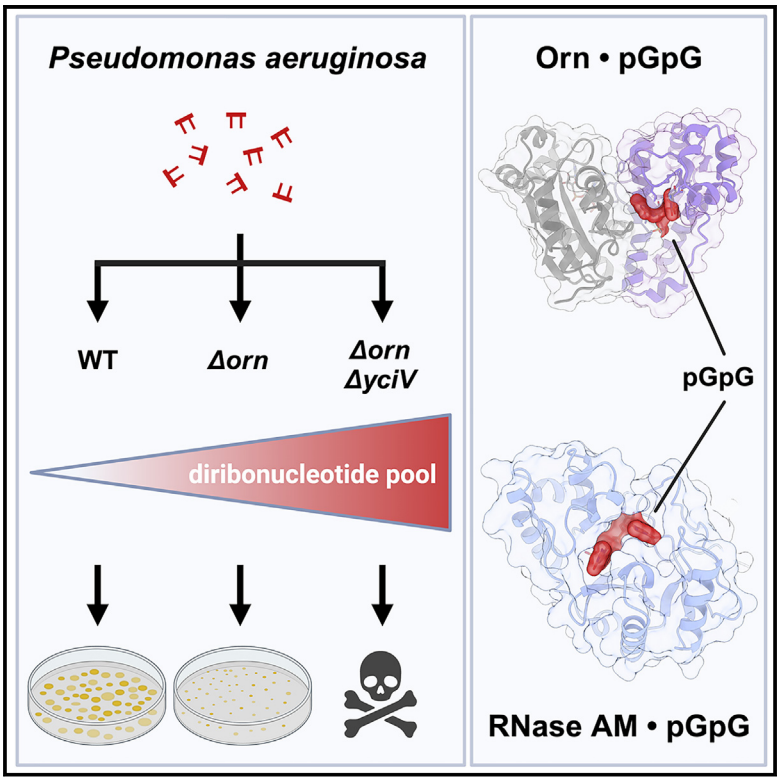

Authors

Soo-Kyoung Kim, Mona W. Orr, Husan Turdiev, ..., Holger Sondermann, Wade C. Winkler, Vincent T. Lee

Correspondence

vtlee@umd.edu

In brief

Orn is a diribonuclease that is essential in some γ-proteobacteria but not *Pseudomonas aeruginosa.* Using genetic screens in *P. aeruginosa*, Kim et al. identified that *yciV*, which encodes RNase AM, has dinuclease activity that is sufficient to prevent lethality. The results indicate that the removal of diribonucleotides is an essential function in γ-proteobacteria.

Highlights

- Small colony phenotype in *Δorn* can be rescued by expression of *yciV*, which encodes RNase AM
- RNase AM is a 5′ to 3′ exoribonuclease that can cleave diribonucleotides
- *P. aeruginosa* RNase is more active than RNase AM from other γ-proteobacteria
- γ-Proteobacteria require diribonuclease to prevent toxic diribonucleotide accumulation

Kim et al., 2024, Cell Reports *43*, 114759
September 24, 2024
https://doi.org/10.1016/j.celrep.2024.114759

CellPress

Cell Reports

CellPress
OPEN ACCESS

Article

Diribonuclease activity eliminates toxic diribonucleotide accumulation

Soo-Kyoung Kim,[1,4] Mona W. Orr,[1,5] Husan Turdiev,[1] Conor C. Jenkins,[1] Justin D. Lormand,[2] Tanner M. Myers,[1] Audrey Andy Burnim,[3] Jared.A. Carter,[1] Warren C. Kung,[1] Xiaofang Jiang,[3] Holger Sondermann,[2] Wade C. Winkler,[1] and Vincent T. Lee[1,6,*]

[1]Department of Cell Biology and Molecular Genetics, University of Maryland at College Park, College Park, MD 20742, USA
[2]CSSB Centre for Structural Systems Biology, Deutsches Elektronen-Synchrotron DESY, 22607 Hamburg, Germany
[3]Intramural Research Program, NLM, NIH, Bethesda, MD 20894, USA
[4]Research Institute for Drug Development, Pusan National University, Busan 46241, South Korea
[5]Present address: Biochemistry & Biophysics Program, Amherst College, Amherst, MA 01002, USA
[6]Lead contact
*Correspondence: vtlee@umd.edu
https://doi.org/10.1016/j.celrep.2024.114759

SUMMARY

RNA degradation is a central process required for transcriptional regulation. Eventually, this process degrades diribonucleotides into mononucleotides by specific diribonucleases. In *Escherichia coli*, oligoribonuclease (Orn) serves this function and is unique as the only essential exoribonuclease. Yet, related organisms, such as *Pseudomonas aeruginosa*, display a growth defect but are viable without Orn, contesting its essentiality. Here, we take advantage of *P. aeruginosa orn* mutants to screen for suppressors that restore colony morphology and identified *yciV*. Purified YciV (RNase AM) exhibits diribonuclease activity. While RNase AM is present in all γ-proteobacteria, phylogenetic analysis reveals differences that map to the active site. RNase AM_{Pa} expression in *E. coli* eliminates the necessity of *orn*. Together, these results show that diribonuclease activity prevents toxic diribonucleotide accumulation in γ-proteobacteria, suggesting that diribonucleotides may be utilized to monitor RNA degradation efficacy. Because higher eukaryotes encode Orn, these observations indicate a conserved mechanism for monitoring RNA degradation.

INTRODUCTION

Since the discovery of RNase A,[1] numerous studies have sought to identify enzymes that complete the turnover of RNA polymers into mononucleotides. One set of early studies biochemically identified and named oligoribonuclease (Orn) because the enzyme degraded RNA oligoribonucleotides from two to five nucleotides to mononucleotides.[2–4] The view that one enzyme processes all short RNA oligoribonucleotides has been accepted for prokaryotic and eukaryotic systems.[5–9] The gene encoding *orn* was subsequently discovered in *Escherichia coli* and revealed to be essential,[10] which is unique among all other exoribonucleases. Three mechanisms have been proposed to explain the essentiality of *orn*: (1) loss of *orn* leads to depletion of mononucleotides, (2) accumulation of oligoribonucleotides is toxic to cells, or (3) an unknown moonlighting activity of Orn is essential. Which of these mechanisms is the basis for essentiality remained unsolved.

A separate line of study reported that the bacterial second messenger cyclic-di-guanosine monophosphate (c-di-GMP) is degraded through a two-step process in which the cyclic nucleotide is linearized into a pGpG diribonucleotide by one set of enzyme(s) and then hydrolyzed to two GMPs by another set of enzyme(s).[11] The enzyme responsible for linearizing c-di-GMP, an EAL domain-containing protein, was identified first.[12] The enzyme required for hydrolyzing pGpG was identified later as Orn in two independent studies using *Pseudomonas aeruginosa*,[13,14] enabled by the fact that for unknown reasons, a transposon insertion mutant of *orn* was viable in *P. aeruginosa*.[15] A study that tested all other known 3′ to 5′ exoribonucleases in *P. aeruginosa* showed that only Orn from this organism, or functionally equivalent nano-RNases from other bacterial species, could cleave pGpG.[16] Taken together, these studies suggested that Orn cleaves diribonucleotides.

However, we wondered how Orn differentiates between these diribonucleotides and oligoribonucleotide substrates of different lengths and avoids acting on longer RNA molecules, which would sequester the enzyme from the short substrates. We were surprised to discover that purified Orn has a more than 100-fold preference for diribonucleotides over longer substrates.[17] For example, in *ex vivo* experiments, a 7-nt-long RNA was degraded by *P. aeruginosa* lysates into mononucleotides, whereas the lysates of Δ*orn* accumulated diribonucleotides.[17] The molecular basis of the stark selectivity of Orn for diribonucleotides was revealed by the co-crystal structure of Orn and diribonucleotides. The structures revealed that Orn has a highly restricted substrate-binding site that also serves as the catalytic site. This substrate binding pocket consists of a surface

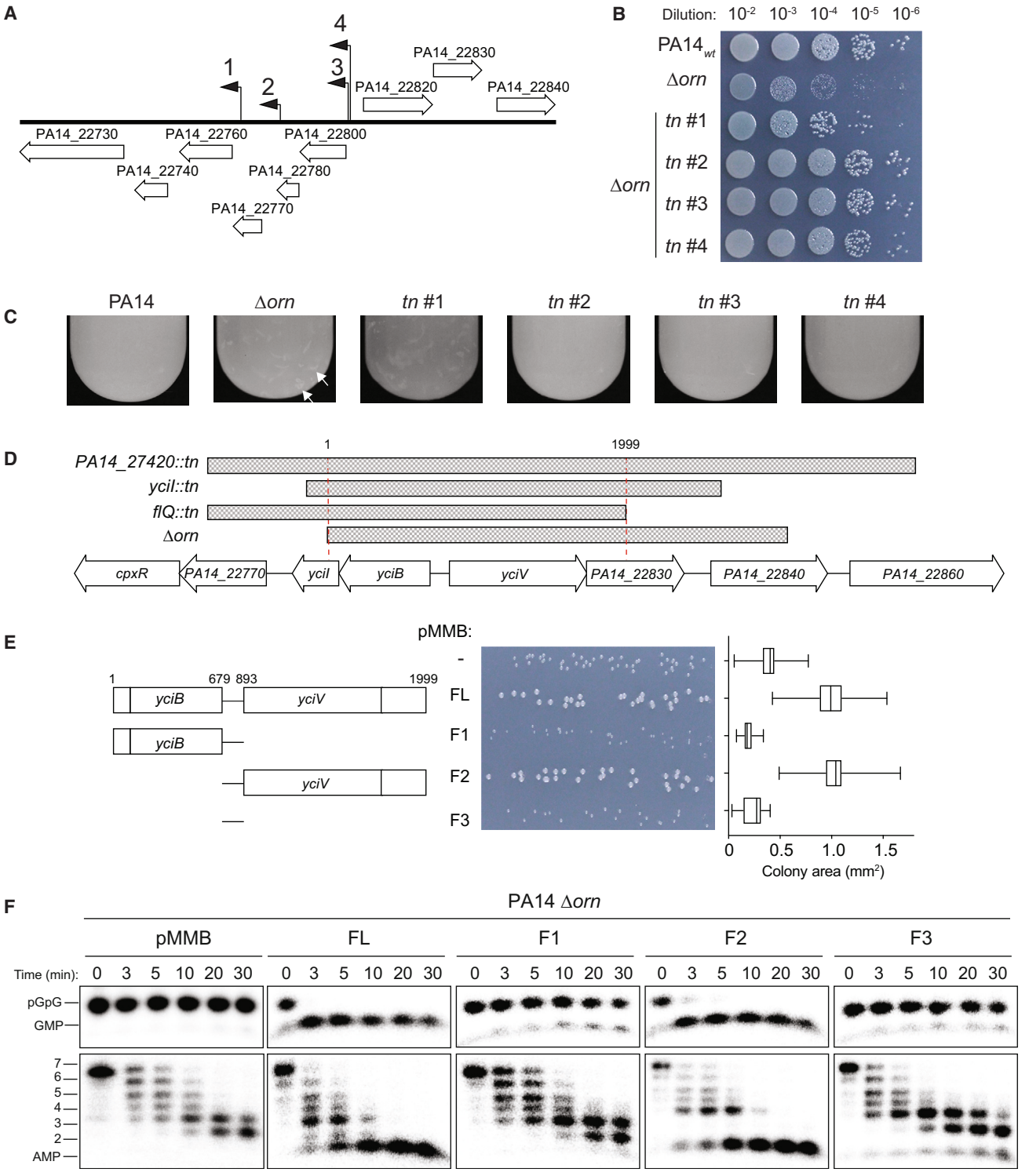

Figure 1. Transposon suppressor screen and complementation of suppressor for restoration of *Δorn* colony size identified *yciV*

(A) Map of the transposon insertions. Tn #1 is in *cpxR* (PA14_22760), Tn #2 is in *yciI* (PA14_22780), and Tn #3 and #4 are in *yciB* (PA14_22800).

(B) Photograph of plates showing in colony size of transposon suppressor mutant compared to PA14 and PA14 Δ*orn*.

(C) Photograph of tubes containing overnight culture of transposon mutant, PA14, and PA14 Δ*orn* for visualization of bacterial aggregates.

(D) The genomic region surrounding the transposon insertion sites.

(legend continued on next page)

patch that selects for the 5′ phosphate, a leucine wedge to orient the diribonucleotide substrate for cleavage, and a flexible loop that moves the catalytic histidine in place; together, these conserved features determine the high selectivity of Orn for diribonucleotides.[17]

The discovery that Orn only cleaves diribonucleotide substrates led us to revisit the basis for essentiality of *orn* in γ-proteobacteria. When Orn was thought to cleave oligoribonucleotides of all lengths, the absence of Orn would have resulted in the sequestration of many nucleotides in these oligonucleotide fragments, and it could be assumed that cells would be depleted of monoribonucleotides. However, because Orn predominantly cleaves diribonucleotides, the degradation of long RNA molecules (mRNA, rRNA) should release the majority of the molecule as mononucleotides by other exoribonucleases, and only the 5′ end of each RNA fragment will become diribonucleotides. The reason why *orn* is essential as a diribonuclease is unclear.

To improve our understanding of *orn*'s essentiality, we took advantage of the fact that *P. aeruginosa* Δ*orn* is viable but exhibits a small-colony phenotype. In this study, we obtained suppressor mutants that restored the colony morphology to wild-type levels. These suppressor strains featured alterations of the *yciV* gene. The *yciV* gene encodes an enzyme with a polymerase and histidinol phosphatase (PHP) domain and has been reported to cleave short oligonucleotides. Indeed, we found that purified YciV acts as a 5′-3′ exoribonuclease that can act on short nucleic acid substrates. Yet, YciV is found in the genomes of many γ-proteobacteria, including *E. coli*. So, if YciV contributes to the survival of the *P. aeruginosa* Δ*orn* strain, why does it not assist with the survival of an *E. coli* Δ*orn* strain as well? Through a combination of biochemical studies, structural characterization, and bioinformatic analyses, we found that *P. aeruginosa* YciV has unique residues in its catalytic site that specifically correlate with increased cleavage of diribonucleotide substrates. Since the only suppressor of Δ*orn* is *yciV*, these results suggest that diribonucleotides are biologically active molecules that have adverse effects if they accumulate in the cell. Additional proteomic studies show that cells have low levels of Orn and YciV and suggest that diribonucleotides are recognized in the cell as a mechanism to monitor the RNA degradation process.

RESULTS

A transposon mutagenesis screen of suppressor mutants for the restoration of colony size

To identify other genes involved in the small colony variant (SCV) phenotype observed in the *Δorn* strain, a suppressor screen was carried out using transposon mutagenesis to identify mutants that would restore *Δorn* colony size to that of the wild type. A pBT20 plasmid containing a mini-mariner-based transposon was introduced into *P. aeruginosa* PA14 *Δorn*.[18] Screening approximately 40,000 colonies identified ∼200 that fully or partially restored the Δ*orn* colony size to that of the wild type. A second screen of these initial mutants yielded four insertions that reproducibly restored colony size. When the transposon from each strain was cloned and sequenced, they mapped to the same genomic region, including one insertion in *PA14_22770,* one insertion in *PA14_22780*, and two insertions in the intergenic region between *PA14_22800* and *PA14_22820* (Figure 1A). To determine the level of suppression, the suppressor strains were plated on lysogeny broth (LB) agar plates to determine colony size. They were also grown overnight in liquid culture to assess aggregation, as it was previously shown that *P. aeruginosa* Δ*orn* is prone to aggregation in liquid medium.[14] All four suppressor strains restored the colony size of *Δorn* to the parental PA14 colony size (Figure 1B). Similarly, the four transposon insertion mutations fully or partially suppressed the aggregation phenotype (Figure 1C). To assess whether the insertion of the transposons into the particular location disrupted the expression of *PA14_22770*, *PA14_22780*, and *PA14_22800*, in-frame deletion mutations of each gene were generated in combination with Δ*orn*. Surprisingly, in-frame deletion of these genes in the *Δorn* background failed to recapitulate the suppression of the small colony size and aggregation observed for transposon insertions (Figures S1A and S1B). These findings indicated that the genes disrupted by the transposon insertion were not responsible for the observed suppression.

Overlapping genomic fragment containing genes disrupted by transposons restores colony size of *Δorn* to that of PA14 wild type

We reasoned that a complementation approach could be used to identify the genes responsible for the suppression of the *Δorn* SCV phenotype. Genomic libraries were prepared for the *Δorn* transposon suppressor strains by fragmenting their genomic DNA with a limited AluI digest and cloning these fragments into a plasmid. The genomic libraries were then conjugated into *Δorn* and tested for colony size restoration. We screened approximately 240,000 colonies on eight independent experiments and identified hundreds of colonies with increased colony size (Figure S2A). A secondary screen was conducted to identify strains that grew like wild-type PA14 in liquid medium (Figure S2B, red box). This approach allowed the identification of suppressors in each genomic library. Sequencing of these suppressor plasmids revealed a common genomic region shared among all suppressed strains (Figure 1D). Surprisingly, even the same genomic fragment from Δ*orn* was able to suppress the SCV phenotype of *orn* (Figure 1E). The shared gDNA region containing the full-length fragment (FL, which includes the *ycil*, intergenic region, *yciB*, *PA14_22820*, and *PA14_22830*) was cloned and tested for suppression of Δ*orn*. This common fragment suppresses the SCV phenotype of Δ*orn* (Figure 1E, FL). To determine which genes were required

(E) Photograph of colony size expressing indicated gene fragments in *Δorn*. Bacterial cultures were diluted and dripped on LB agar plate containing carbenicillin for 30 h. The quantification of colony sizes is shown on the plot.

(F) Degradation of AAAAAGG or pGpG by *Δorn* complemented with suppressor fragments. ^{32}P-pGpG (top, 1 μM total) and ^{32}P-AAAAAGG (bottom, 1 μM total) by whole-cell lysates of *Δorn* complemented with indicated gene fragments. Samples were stopped at the indicated time (min) and analyzed by 20% denaturing PAGE.

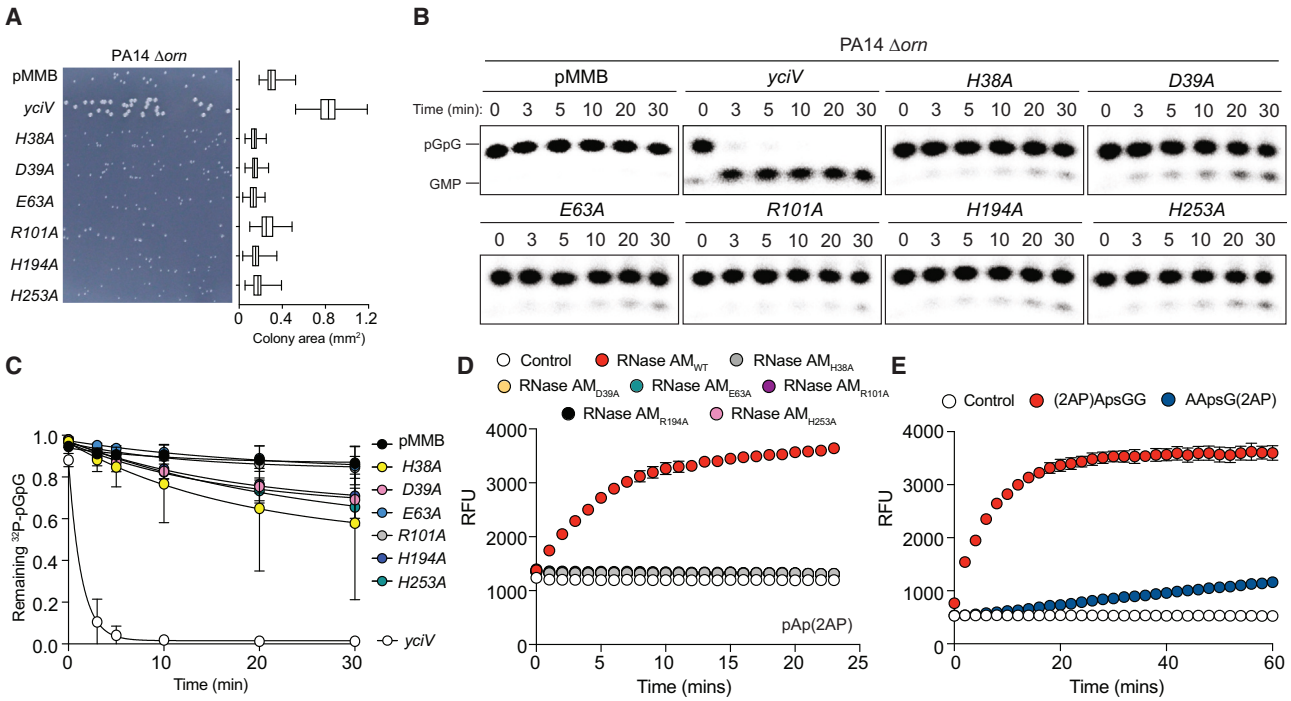

Figure 2. Catalytic site residues of *yciV* are required for diribonuclease activity

(A) Photograph of PA14 Δ*orn* expressing *yciV* or alanine substitution alleles were grown on LB agar plate containing 1 mM IPTG for 30 h. Graph shows colony size as measured by Fiji software.

(B) Degradation of ^{32}P-pGpG (total 1 μM) by whole-cell lysates PA14 Δ*orn* complemented with *yciV* or variants at indicated alanine substitutions was assessed. Samples are stopped at the indicated times (min) and analyzed by 20% denaturing PAGE. All data shown represent the average of triplicate independent experiments.

(C) The graph shows the quantification of triplicate data by the amount of remaining pGpG shown in (B).

(D) Cleavage of pAp(2AP) by purified RNase AM$_{Pa}$ or RNase AM$_{Pa}$ with indicated alanine substation.

(E) Cleavage of (2AP)ApsGG and AApsG(2AP) by purified RNase AM$_{Pa}$ shows that RNase AM$_{Pa}$ is a 5′ to 3′ exonuclease. For control samples, enzyme was not added.

to mediate suppression, several subfragments were generated: F1 (intergenic region with *yciB*), F2 (intergenic region with *PA14_22820* and *PA14_22830*), and F3 (intergenic region). Only F2 restored normal colony size and growth to that of the wild type, whereas F1 and F3 failed to complement the *Δorn* phenotype (Figure 1E), suggesting that *PA14_22820* is the gene responsible for complementation. We hypothesized that the restoration of colony size and growth might be due to the degradation of accumulated diribonucleotides by *Δorn* complemented by FL and F2. To test this hypothesis, lysates were generated from *P. aeruginosa* strains, including *Δorn* complemented with the vector control, FL, F1, F2, and F3. Each lysate was mixed with 5′-^{32}P-radiolabeled pGpG or pAAAAAGG, and aliquots were taken at the indicated time intervals (Figure 1F). FL and F2 in *Δorn* lysates were able to degrade pGpG into GMP, whereas F1 and F3 failed to complete the degradation of pGpG (Figure 1F, top). Furthermore, 5′-^{32}P-AAAAAGG was degraded into mononucleotides by FL and F2 in *Δorn* lysates, whereas lysates of F1 and F3 in *Δorn* accumulated intermediate diribonucleotides (Figure 1F, bottom). Taken together, these results show that the expression of *PA14_22820* leads to the degradation of pGpG and pApA diribonucleotides in *Δorn* lysates and the restoration of Δ*orn* growth.

The catalytic activity of *PA14_22820* (*yciV*) is required for suppression of the Δ*orn* phenotype and degradation of diribonucleotides

The F2 fragment consists of an intergenic region, full-length *PA14_22820*, and partial *PA14_22830*. We investigated whether *PA14_22820* alone was sufficient to complement the SCV phenotype of *Δorn*. Complementation of *Δorn* with *PA14_22820* under an isopropyl-β-1-D-thiogalactopyranoside (IPTG)-inducible plasmid restored normal colony sizes, in contrast to the vector control (Figure 2A). *PA14_22820* (*yciV*) encodes a protein containing a PHP domain and was previously renamed RNase AM as an enzyme that cleaves ribo- and deoxyribo-oligonucleotides from the 5′ to 3′ direction with enhanced activity toward 3′,5′-pAp and less activity toward longer substrates in *E. coli*.[19] The lysates in *Δorn* complemented with *yciV* were capable of cleaving pGpG into GMP, similar to what was observed for the F2 activity (Figures 2B and 2C). To understand the features of RNase AM that enable the cleavage of diribonucleotides, RNase AM$_{Pa}$ was aligned to the RNase AM sequence from *Chromobacterium violaceum*, *E. coli*, *Vibrio cholerae*, *Salmonella enterica*, and *Yersinia pseudotuberculosis* (Figure S3). We identified multiple residues near the AMP-binding site (H38, D39, E63, H194, and H253) and

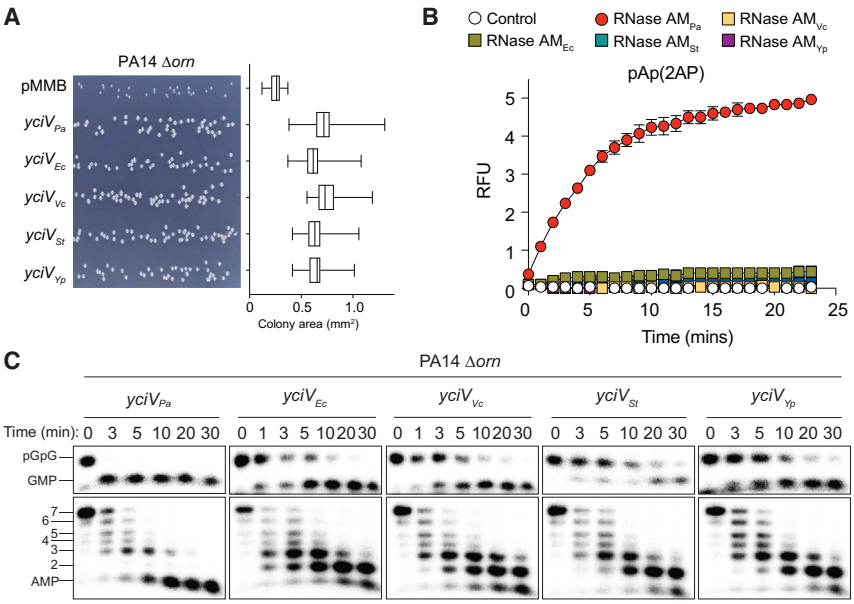

Figure 3. RNase AM homologs from different γ-proteobacteria have reduced diribonuclease activity

(A) Photograph of PA14 Δ*orn* expressing *yciV* from indicated γ-proteobacteria were grown on LB agar plate containing 1 mM IPTG for 30 h. Graph shows colony size as measured by Fiji software.

(B) Cleavage of pAp(2AP) by purified RNase AM orthologs from γ-proteobacteria.

(C) Degradation of ^{32}P-pGpG (top) or ^{32}P-AAAAAGG by whole-cell lysates PA14 Δ*orn* expressing *yciV* from indicated γ-proteobacteria was assessed. Samples are stopped at the indicated times (min) and analyzed by 20% denaturing PAGE. All data shown represent the average of triplicate independent experiments.

phosphate-binding site (R101) in the *C. violaceum* structure[19] and introduced alanine substitution mutations into the corresponding residue in RNase AM$_{Pa}$. To determine the activity of these mutant alleles, we tested their ability to increase the colony size of Δ*orn*, an effect indicative of diribonuclease activity. While *yciV*^{WT} suppressed Δ*orn* with an average colony size of 0.8 mm^2, the mutant alleles of *yciV* failed to restore colony size (Figure 2A). When lysates from *Δorn* expressing these variants were tested for their ability to degrade pGpG into GMP, none of the alanine substitution variants had activity comparable to that of wild-type *yciV* (Figures 2B and 2C). Taking these results together, RNase AM suppression of the colony size of *Δorn* strains appears to require the cleavage of diribonucleotides.

RNase AM$_{Pa}$ is a 5′ to 3′ oligoribonuclease

To determine whether RNase AM$_{Pa}$ alone can cleave diribonucleotides, RNase AM$_{Pa}$ protein was purified and tested for activity against 2-aminopurine (2AP)-containing oligonucleotide substrates. 2AP released from oligonucleotides exhibits enhanced fluorescence.[20] Purified RNase AM$_{Pa}$ was able to cleave pAp(2AP), but all variants with active site alanine substitutions failed to cleave the same substrate, supporting our findings with radiolabeled substrates (Figure 2D). To determine whether RNase AM$_{Pa}$ also cleaves from the 5′ end, we utilized two substrates that were 4 nt long with a non-hydrolyzable phosphothioate linkage between the second and third nucleotides. For one substrate, the 2AP is the first base at the 5′ end and allows detection of 5′ cleavage of the substrate. For the other substrate, 2AP is the last base at the 3′ end and allows the detection of 3′ cleavage of the substrate. Purified RNase AM$_{Pa}$ was only able to release 2AP from the 5′ end but not the 3′ end (Figure 2E). These results indicate that RNase AM$_{Pa}$ cleaves short oligoribonucleotides of various lengths from the 5′ end.

SCV and diribonucleotide degradation activity are partially restored by RNase AM orthologs

Orn is essential in many γ-proteobacteria but not *P. aeruginosa*, where *Δorn* has an SCV morphology. We asked if the different requirement for *orn* is due to the other γ-proteobacteria not encoding *yciV*. Notably, RNase AM orthologs are present in *E. coli*, *V. cholerae*, and *Y. pestis*, for all of which *orn* has been reported to be essential.[10,21,22] To determine whether the reason for *orn* essentiality is due to species-specific differences in the function or activity of these enzymes, RNase AM orthologs were expressed in *P. aeruginosa Δorn* and assessed for restoration of normal growth and colony morphology. Surprisingly, all RNase AM orthologs, including RNase AM$_{Ec}$, RNase AM$_{Vc}$, RNase AM$_{St}$, and RNase AM$_{Yp}$, were able to suppress small colony morphology in a similar manner to RNase AM$_{Pa}$ (Figure 3A).

When the purified proteins were tested for the degradation of diribonucleotides, only RNase AM$_{Pa}$ was able to effectively cleave the pAp(2AP) diribonucleotide, whereas the orthologs from other γ-proteobacteria had little activity (Figure 3B). To understand the activity of RNase AM in cells, we tested lysates from *Δorn* cells expressing each of the RNase AM orthologs for the degradation of ^{32}P-labeled pGpG and AAAAAGG. While the expression of RNase AM$_{Pa}$ in *Δorn* allowed complete cleavage of pGpG into GMP within 5 min, other RNase AM orthologs showed slower degradation over time: RNase AM$_{Ec}$ and RNase AM$_{Vc}$ required 30 min to degrade pGpG, whereas RNase AM$_{St}$ and RNase AM$_{Yp}$ were unable to cleave all of the pGpG within 30 min (Figure 3C). For the 7-mer substrate, *P. aeruginosa* Δ*orn* has been shown to accumulate 5′ diribonucleotides, indicating that other 3′ exoribonucleases can degrade RNA to diribonucleotides (Figure 1F, bottom).[17] The expression of RNase AM$_{Pa}$ allowed the completion of the degradation of the accumulated diribonucleotide to mononucleotide (Figure 3C). When RNase AM from *E. coli*, *V. cholerae*, *S. enterica*, and *Y. pseudotuberculosis* were overexpressed, less than 50% of the diribonucleotides were cleaved to mononucleotides. To better understand whether there were differences in substrate preference for these different orthologs of RNase AM, the lysates of

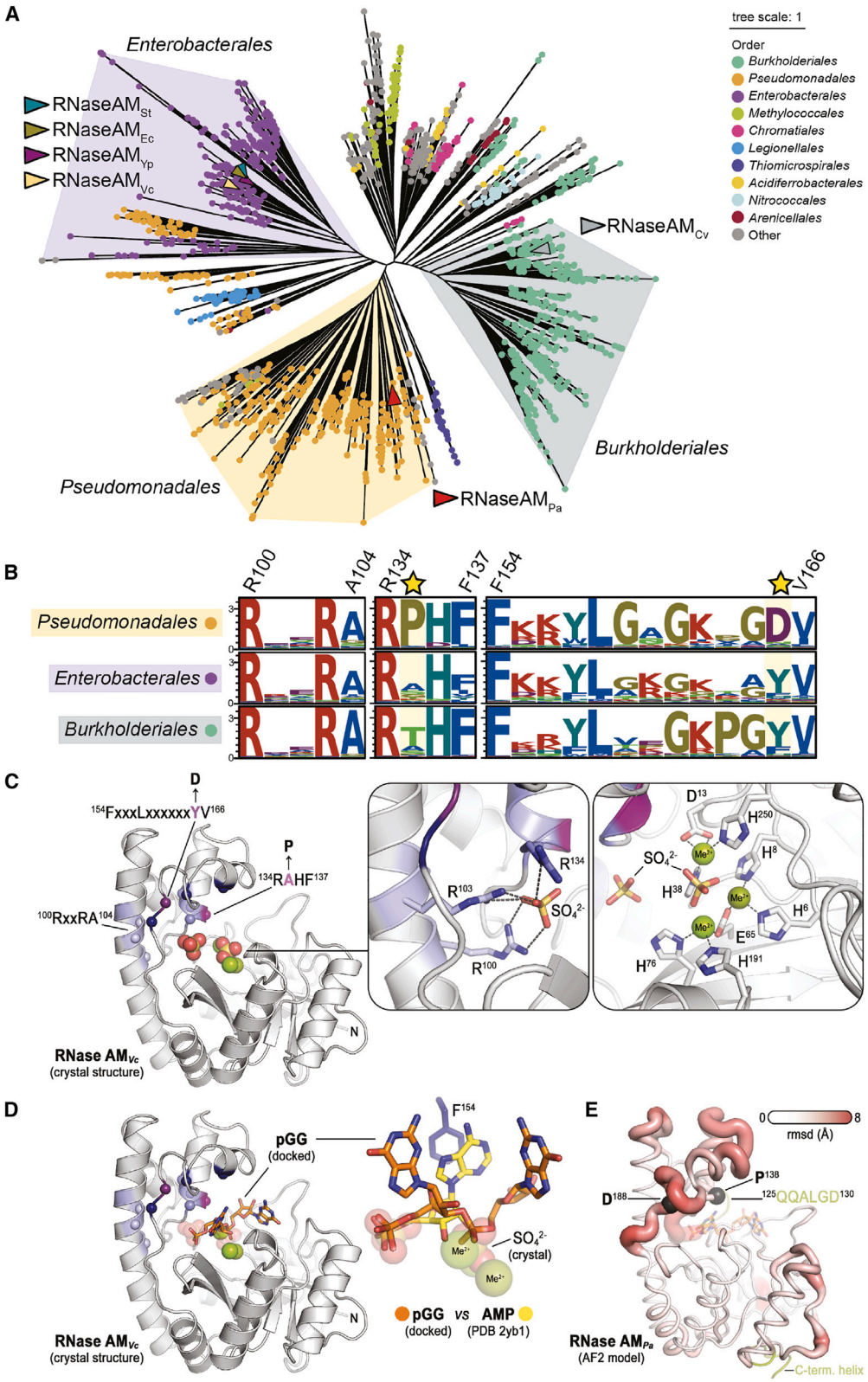

(legend on next page)

Δ*orn* expressing each of the *yciV* orthologs were tested for activity against all 16 diribonucleotides. Previously, Orn has been reported to degrade all 16 diribonucleotides.[17] The lysates of *Δorn* expressing RNase AM_{Pa} were able to degrade >50% of diribonucleotides except for pApA, pCpC, pUpU, pUpA, and pUpC (Figure S4). In contrast, lysates of *Δorn* expressing RNase AM_{Ec}, RNase AM_{Vc}, RNase AM_{St}, and RNase AM_{Yp} proficiently processed a subset of diribonucleotides, whereas the remaining diribonucleotides were poor substrates. The diribonucleotide substrates included pApG and pGpU by RNase AM_{Ec}; pApG, pApU, pGpG, pGpC, and pGpU by RNase AM_{Vc}; pGpG and pGpC by RNase AM_{St}; and pGpG by RNase AM_{Yp}. These results indicate that RNase AM_{Pa} has a narrower substrate spectrum than Orn. However, orthologs from other γ-proteobacteria have even lower activity and more restricted substrate profiles, distinguishing them from RNase AM_{Pa}.

Unique residues of RNase AM_{Pa} located near the active site of the enzyme

These results led us to investigate whether there are unique features of RNase AM_{Pa} that differ from orthologs found in other γ-proteobacteria. Phylogenetic analysis of RNase AM orthologs identified 1,621 RNase AM sequences between 200 and 400 amino acids. Several groups were identified when clustered by relatedness, including a group consisting of Pseudomonadales (yellow in Figure 4A), Enterobacterales (purple in Figure 4A), and Burkholderiales (green in Figure 4A). A comparison of the logos generated for sequences near the catalytic site for each group revealed key residues that were highly conserved and two residues that distinguished the groups (Figure 4B). In particular, RNase AM from Pseudomonadales has two key residues, P^{135} and D^{165}, which differ from the corresponding residues in Burkholderiales and Enterobacterales.

Next, we sought structural insights into the substrate specificity of RNase AM orthologs. Although RNase AM_{Pa} has resisted crystallization to date, we were able to determine the crystal structure of full-length RNase AM from *V. cholerae*, RNase AM_{Vc}, at a maximum resolution of 1.5 Å (Figure 4C). The electron density resolved the entire sequence from residues 1 to 279, with the last 11 residues of the protein being disordered. RNase AM was incubated with excess pGpG prior to crystallization, yet no nucleotide density was discernible at the active site. However, the active site contained three divalent cations (Mg^{2+} or Mn^{2+}), which are coordinated by strictly conserved residues, and two sulfate ions from the crystallization buffer (Figure 4C, insets). One of the sulfate ions is coordinated by the metal ions instead of the protein, likely mimicking the scissile phosphodiester of a substrate. The presence of divalent cations, which are crucial for catalytic activity, and solvent molecules, which can compete for substrate binding, may explain the lack of bound substrates in the crystals. A comparison with known experimentally determined structures using a Foldseek search identified *E. coli* (PDB: 7UG9[23]) and *C. violaceum* (PDB: 2YB1[24]) RNase AM as close structural orthologs, despite having only 43% and 40% sequence identity, respectively.[25] A phosphoesterase from *Bifidobacterium adolescentis* also shows a high degree of structural homology, but its sequence identity is less than 30% (PDB 3E0F[26]). While the structure of RNase AM_{Ec} represents the closest ortholog of RNase AM_{Vc} with a known structure and the two structures align with a root-mean-square deviation (RMSD) of 0.6 Å over 190 Cα positions, the insertion lobe that contains the residues distinguishing the different groups of RNase AM sequences was not resolved in the structure of the *E. coli* protein. The structures of RNase AM_{Cv} and *B. adolescentis* phosphoesterase resolve this region and align to RNase AM_{Vc} with RMSD values of 1.2 and 1.8 Å, respectively, but belong to distinct phylogenetic orders.

Since there are no reported crystal structures of RNase AM with bound substrates, we docked pGpG against the crystal structure of RNase AM_{Vc} employing the DiffDock method.[27,28] In addition to a moderate confidence score (−0.83 for the top-ranking model), the solution places the phosphate groups of the diribonucleotide, where two sulfate ions are resolved in the crystal structure (Figure 4D). Consequently, the scissile phosphodiester is in close proximity to the three metal ions at the active site of RNase AM. Furthermore, the 5′ phosphate is in a position comparable to that of AMP in the crystal structure of RNase AM_{Cv}.[24] The residue F^{154} of RNase AM_{Cv}, which is strictly conserved in the RNase AM family, forms a π-stacking interaction with the AMP base. Although the corresponding residue of

Figure 4. RNase AM structure and key sequences

(A) Phylogenetic tree and key sequence conservation of RNase AM proteins. Shown is an unrooted phylogenetic tree of RNase AM sequences, with sequences of interest highlighted by triangles on the branch tips. The branch tips are colored by taxonomic order for the organism for each RNase AM sequence, with the color key shown to the right. Only the top 10 most populated taxonomic orders are shown for clarity; all others are in gray. The major clades are labeled by the most representative taxonomic order. Only the top 10 most populated taxonomic orders and top 18 taxonomic families are shown for clarity; all others are in gray.

(B) Sequence logos for major clades in the RNase AM phylogeny. Each logo shows the information entropy of important sequence motifs. The residue numbering for *Pseudomonas aeruginosa* is shown labeled on top of the sequences. Stars highlight conservation in the Pseudomonadales clade that is not conserved in Enterobacterales or Burkholderiales.

(C) Crystal structure of RNase AM_{Vc}. The cartoon shows the structure of *V. cholerae* RNase AM bound to divalent metal ions and two sulfate molecules (shown here as spheres) at the active site. Close-up views highlight key residues that interact with the ligands. The conserved sequence features shown in (B) are labeled and colored in blue or purple.

(D) Predicted diribonucleotide-binding site and pose. Computational docking of pGpG to the crystal structure of RNase AM_{Vc} resulted in a top-ranked solution in which the diribonucleotide was placed at the active site of the enzyme. Ligands from the crystallization are shown as transparent spheres. The inset shows a close-up view of the docking solution and crystallographic ligands, in addition to AMP from the crystal structure of RNase AM_{Cv} (PDB: 2YB1). The side chain of residue F^{154} in RNase AM_{Vc} is shown as sticks.

(E) Structural model of RNase AM_{Pa}. The AF2 model of *P. aeruginosa* RNase AM was aligned with the crystal structure of RNase AM_{Vc}. The model is shown as a cartoon putty, with the putty thickness and color gradient indicating the RMSD between corresponding residues. An insertion and a predicted C-terminal helix in RNase AM_{Pa} is shown and labeled in light green. The positions of Pseudomonadales-specific sequence changes are highlighted as black spheres representing their corresponding Cα positions.

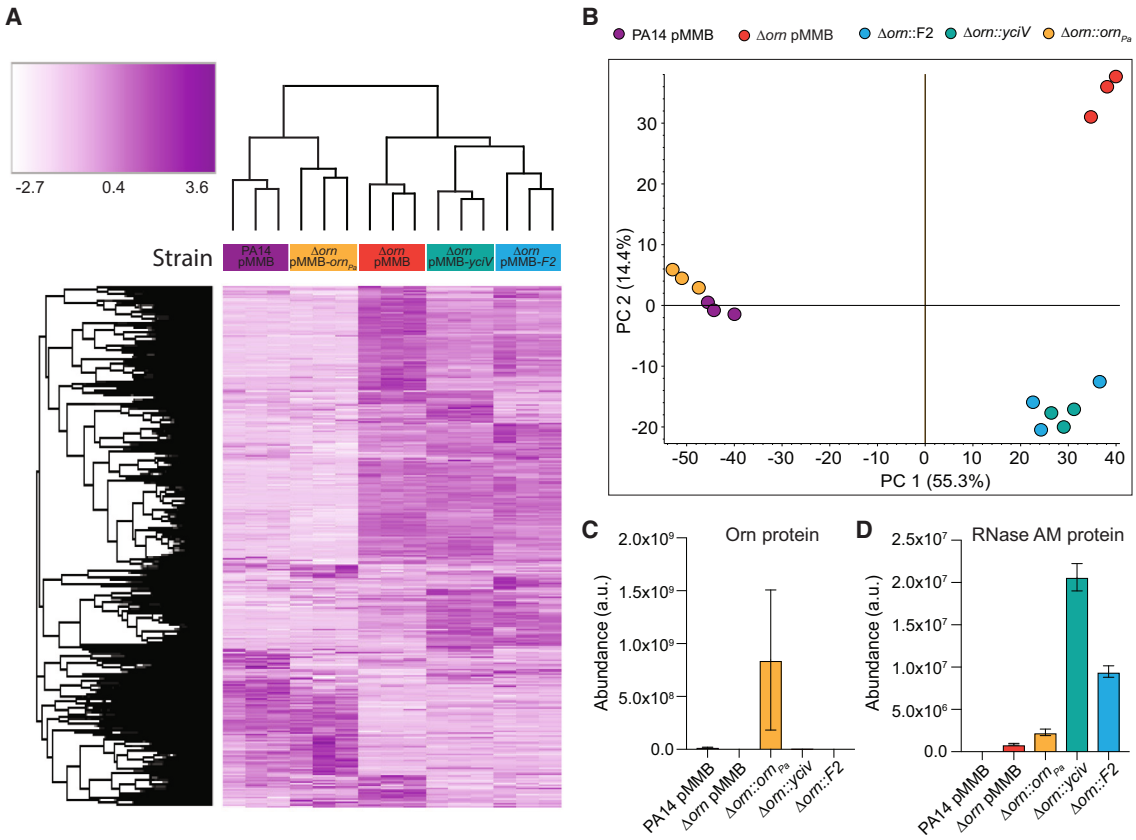

Figure 5. Proteomic analysis of *P. aeruginosa* Δ*orn* and complemented strains

(A) Normalized protein abundances of each sample (x axis) and each protein (y axis) are clustered by Euclidean distance with a complete linkage method. The clustering resulted in the grouping of samples relative to strain under two discriminate sub-trees.

(B) A principal-component analysis of the normalized protein abundance data.

(C) A bar graph representing the abundance of Orn_{Pa} in arbitrary units in each strain.

(D) A bar graph representing the abundance of RNase AM_{Pa} in arbitrary units in each strain.

RNase AM_{Vc} exhibits the same rotamer, the bases of the docked pGpG do not overlap with AMP (Figure 4D, inset). Instead, the bases appear splayed. This conformation may allow residue F^{154} to function as a wedge when inserted between the two bases of the diribonucleotide substrate. Such a role would be similar to the leucine wedge observed in Orn and NrnC and could be relevant for the specific activity of these enzymes against diribonucleotides.[17,29] The 3′ side of the docked pGpG faces the periphery of the active site groove, suggesting that there is no strict length preference for 5′-3′ RNase activity.

Mapping the positions of the two residues that are conserved in Pseudomonadales RNase AM sequences but differ in all other groups, P^{135} and D^{165}, onto the structure of RNase AM_{Vc} illustrated their proximity to the active site of the enzyme (Figures 4C and 4D). In addition, we modeled the structure of RNase AM_{Pa} by using AF2 and ColabFold[30,31] (Figure 4E). The high-confidence model predicted a short insertion in the active-site-proximal lobe and a C-terminal helix in the *P. aeruginosa* model, both of which are missing from the corresponding structure of the *V. cholerae* homolog. The RNase AM_{Pa} model superimposes well with the crystal structure of RNase AM_{Vc}, aligning with an average RMSD of 1.1 Å. However, closer inspection of the superposition revealed higher RMSD values for residues in the aforementioned lobe than for those of the domain containing the catalytic core of the enzyme (Figure 4E). The Pseudomonadales signature residues are part of this lobe. It is conceivable that the unique features of this group of RNase AM enzymes collectively or individually contribute to the shifted higher activity of RNase AM_{Pa} toward diribonucleotides.

Low levels of Orn and RNase AM in *P. aeruginosa* suggest that diribonuclease activity is limited

Since *P. aeruginosa* encodes both *orn* and *yciV*, it is unclear why the Δ*orn* mutant has a phenotype when the *yciV* gene is present in the genome. To better understand this, proteomic analysis was performed on the PA14 vector control, Δ*orn* vector control, Δ*orn* pMMB-F2, Δ*orn* pMMB-orn_{Pa}, and Δ*orn* pMMB-$yciV_{Pa}$. Global protein expression profiles were investigated using Euclidian-based clustering at the sample and individual protein levels (Figure 5A). At the strain level, individual biological replicates grouped closely into their individual

strains. The Δ*orn* and PA14 strains have distinctive proteomes clustered into two groups: proteins increasing in abundance and proteins decreasing in abundance upon *orn* knockout. Upon complementation with *orn*, the proteome was restored to wild-type levels. Conversely, complementation with either the F2 fragment or $yciV_{Pa}$, while restoring colony size and diribonucleotide cleavage, did not restore global proteome levels. Principal-component analysis (PCA) of these samples showed that Δ*orn* had a very different proteome from PA14 or Δ*orn* complemented with orn_{Pa} (Figure 5B). In contrast, the expression of the F2 fragment or $yciV_{Pa}$, while restoring colony size and cleavage of diribonucleotides, yielded a distinct proteome from either PA14 or Δ*orn* (Figure 5B). Within the proteomic data, the protein level of Orn in PA14 was detectable compared to that in Δ*orn*, but Orn appeared to be expressed at a very low level in the wild-type strain (Figure 5C). Complementation with *orn* on a plasmid greatly increased Orn protein levels, which corresponds to the increased diribonuclease activity reported previously.[17] The expression of F2 and $yciV_{Pa}$ in a Δ*orn* genetic background did not affect Orn protein levels, which remained undetectable. Protein expression of RNase AM_{Pa} in wild-type PA14 was undetectable but increased in Δ*orn* (Figure 5D). Complementation with *orn* did not alter RNase AM_{Pa} as compared to Δ*orn* with the vector control. In contrast, F2 and *yciV* expression significantly increased RNase AM_{Pa}. The increased protein levels of RNase AM_{Pa} in Δ*orn* likely explain why Δ*orn* has a phenotype but is viable, as the amount of RNase AM_{Pa} is not high enough to fully complement the activity of Orn but sufficient for the cells to survive the accumulation of diribonucleotides.

Diribonuclease activity appears to be the basis for *orn* essentiality in *E. coli* and *P. aeruginosa*

To reconcile the difference in genetic essentiality of *orn* in *E. coli* and *P. aeruginosa*, two sets of genetic experiments were performed to determine whether the *orn* gene can be deleted from the genome. In the first experiment, *E. coli* TW6 was transformed with an empty pMMB vector and tested for deletion of *orn* by lambda red recombinase.[32–34] When TW6 pMMB was transformed with a PCR product consisting of the chloramphenicol resistance (Cm^R) gene flanked by 50 bp of sequences upstream and downstream of the *E. coli orn* gene, only three Cm^R colonies arose (Figure 6A). When tested by PCR, all three Cm^R colonies had the wild-type *orn* gene, suggesting that the resistance marker was integrated elsewhere in the genome (Figure S6A). When TW6 pMMB-orn_{Pa} was transformed with the same *orn* deletion fragment, 49 Cm^R colonies appeared. PCR testing of 16 of these colonies chosen at random revealed that 13 of them had the orn_{Ec} gene deleted from the chromosome (Figures 6A and S6A). When TW6 pMMB-F2 was transformed with the same *orn* deletion fragment, over 100 colonies appeared. PCR testing of 16 of these colonies chosen at random revealed that 12 of them had the orn_{Ec} gene deleted from the chromosome (Figures 6A and S6A). In contrast, inactive alleles of *orn* or *yciV* failed to generate *orn* deletion mutants (Figures 6A and S6A). These results suggest the essentiality of *orn* in *E. coli* is due to diribonuclease activity of Orn, and this activity can be replaced by RNase AM_{Pa}.

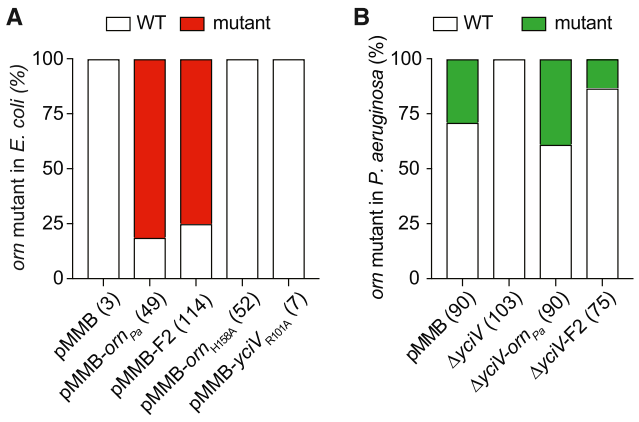

Figure 6. Diribonuclease activity is required in γ-proteobacteria

(A) PCR product was transformed into *E. coli* and orn_{Ec} was replaced with chloramphenicol acetyltransferase gene via lambda red recombination. The number of Cm^R colonies is indicated in parentheses. The number of colonies in which the *orn* gene is substituted with the chloramphenicol acetyltransferase gene was determined by PCR.

(B) *P. aeruginosa* harboring a co-integrant for the Δ*orn* deletion was resolved by growth in the absence of selection followed by counterselection on sucrose. Colonies were assessed by PCR to determine the number of colonies that reverted to wild type or deleted the *orn* gene.

In the second experiment, we generated a co-integrant in PA14 by selecting gentamicin for the integration of a plasmid with an *orn* deletion construct flanked by 1 kb upstream and downstream of *orn* and a gentamicin resistance gene.[14] When grown in the absence of selection, the integrated plasmid can be recombined out to yield either the wild-type or Δ*orn* mutant. After counterselection against the co-integrant, we assessed the frequency with which Δ*orn* arose after the resolution of the co-integrant. PCR analysis of 90 colonies resolved from the PA14 co-integrant showed that 30% were Δ*orn* and 70% returned to wild type. When 103 resolved colonies from a PA14 Δ*yciV* co-integrant were assessed, no Δ*orn* was detected (Figures 6B and S6B). Ninety resolved colonies from the co-integrant in PA14 Δ*yciV* pMMB-orn_{Pa} yielded 40% Δ*orn* and 60% wild type (Figure 6B). Lastly, co-integrants resolved from PA14 Δ*yciV* with pMMB-F2 yielded 15% Δ*orn* genes (Figure 6B). Together, these data indicate that both *E. coli* and *P. aeruginosa* appear to require diribonuclease activity for viability, with *P. aeruginosa* genomes encoding a second enzyme supporting this activity. These results also indicate that the removal of diribonucleotides is an essential process.

DISCUSSION

Orn was initially identified as an oligoribonuclease[2–4] that is essential in *E. coli*.[10] The historical results suggest that the inability to cleave a large array of oligoribonucleotides would result in the depletion of mononucleotides and leave the cell unable to grow. More recently, studies have shown that Orn is the primary enzyme that degrades pGpG to GMP to complete the c-di-GMP signaling cycle.[13,14] Subsequent investigations into why Orn cleaves pGpG revealed that it selectively cleaves

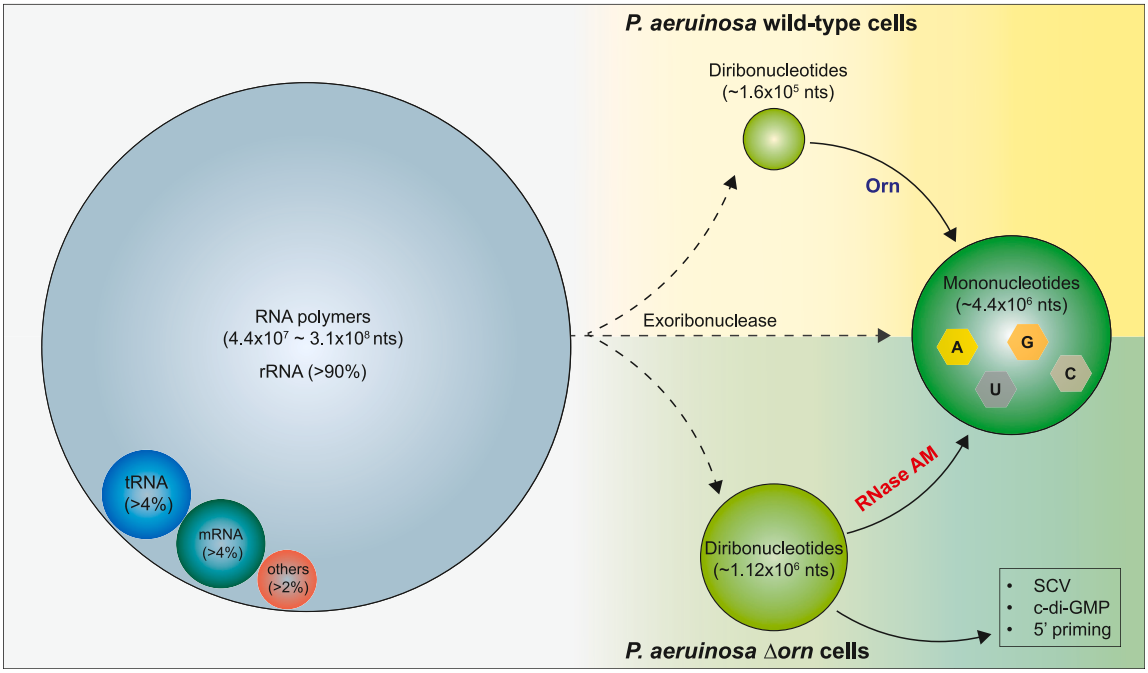

Figure 7. Model for flux of ribonucleotides

Estimate of RNA distribution in growing *P. aeruginosa* cells based on previous studies on *E. coli* and *P. aeruginosa*. The box represents a *P. aeruginosa* cell. The gray area containing circles represents the amount of nucleotides (nt) in each category of RNA that would be present in both genetic backgrounds (wild type [WT] or Δ*orn*). For ribosomes, the amount of nt is based on an estimate of 10,000–70,000 ribosomes in an *E. coli* cell.[35] Each ribosome has ~4,400 nt for a total of ~4.4 × 10^7–3.1 × 10^8 nt. This model uses a cell with 40,000 ribosomes for WT *P. aeruginosa* and Δ*orn*. Each of the mononucleotides (adenine, guanine, cytosine, and uracil) includes mono-, di-, and tri-phosphate versions and has been measured in *E. coli* for a combined total of 5.2 mM.[36,37] In this estimate, there would be ~5.2 × 10^6 nt in the cell as mononucleotides for WT *P. aeruginosa* and Δ*orn*. When degraded, these larger RNA molecules will generate dinucleotides. For WT *P. aeruginosa* (indicated in the yellow portion), Orn is present and will cleave dinucleotides into mononucleotides. A prior estimate of pGpG shows that there is ~10 μM in the cell.[14] Assuming all of the linear diribonucleotides are present at similar concentrations, there would ~160 μM or ~1.6 × 10^5 nt per cell. In Δ*orn* mutants (indicated in the green portion), the concentration of pGpG increases to ~70 μM, which extrapolates ~1.12 × 10^6 nt for all 16 linear dinucleotides per cell.[14]

diribonucleotides over longer oligonucleotides.[17] The co-crystal structure revealed that diribonucleotides fit snuggly into the catalytic site of Orn. Orn has a 5′ phosphate cap and an activation loop that restrict the length of substrate that can enter.[17] While these studies clearly revealed that Orn is a diribonuclease within a cell, they raised questions as to why Orn would be essential, as most of the degraded RNA would be released as mononucleotides by other 3′ to 5′ exoribonucleases and only a small fraction of nucleotides would be sequestered as diribonucleotides (Figure 7). Hence, it is unlikely that depletion of the mononucleotide pool is the reason for the essentiality of *orn*.

To better understand the basis of Orn essentiality, we took advantage of *P. aeruginosa*, an organism in which *orn* mutants were viable despite having a small colony phenotype. Through genetic experiments, we identified RNase AM_{Pa} (previously YciV) as a gene product that can act as a diribonuclease and restore the degradation of diribonucleotides to the Δ*orn* strain. To our surprise, this gene was not unique to *P. aeruginosa* but was also present in other γ-proteobacteria in which *orn* was essential.[19] Phylogenetic analysis revealed that *P. aeruginosa* RNase AM is part of a clade with unique sequences in the catalytic site, which maps to the location of the 5′ base of the diribonucleotide substrate. When assessed for activity, RNase AM_{Pa} was far more active than RNase AM from other γ-proteobacteria. The introduction of RNase AM_{Pa} into *E. coli* permitted the deletion of the *orn* gene from the chromosome. Similarly, removal of the *yciV* gene from *P. aeruginosa* makes the *orn* gene essential.

These results indicate that a minimal level of diribonuclease activity is required in γ-proteobacteria. The diribonuclease activity can be provided by Orn, which is an efficient 3′ to 5′ diribonuclease, or by RNase AM_{Pa}, which is a less efficient 5′ to 3′ oligoribonuclease. Based on the *in vitro* and *ex vivo* results presented here and those reported earlier, Orn is a far more efficient enzyme.[17] RNase AM_{Pa} is more active than RNase AM from other γ-proteobacteria. Despite these differences in activity of RNase AM, overexpression of RNase AM from any γ-proteobacteria restored the normal colony size of Δ*orn*, with higher expression levels likely compensating for the differences in activity profiles. These results provide further support for the existence of a threshold concentration of diribonucleotides in the cell that causes a small colony morphology but is not sufficiently high enough to cause toxicity. In addition, RNase AM_{Pa} is able to suppress the essentiality of *orn* in both *P. aeruginosa* and *E. coli*. Aside from this study, RNase AM_{Ec} is the only known 5′ to 3′ exoribonuclease in *E. coli* that acts to trim three bases from

the 5′ end of 23S RNA.[38] Despite this activity, RNase AM is not essential in *E. coli*, as *yciV* mutants are readily generated and do not have a growth phenotype.[38] The absence of a growth phenotype is likely because helix 1 of 23S RNA, which includes the 5′ processed nucleotides, is not conserved among bacteria and is not required for ribosome function.[39] Since $yciV_{Pa}$ can allow for deletion of *orn* in *E. coli* and the endogenous $yciV_{Ec}$ cannot suggest that the dinuclease activity rather than other functions of RNase AM are required for growth. Because Orn and RNase AM are different in protein sequence, domain structure, and activity (strict diribonuclease vs. a 5′ oligoribonuclease), the basis for essentiality appears to be a requirement for diribonuclease activity.

The essentiality of *orn* has been previously explained by three scenarios.[10] First, the absence of *orn* leads to the accumulation of oligoribonucleotides and the consequent depletion of mononucleotides. Second, oligoribonucleotides inhibit enzymes involved in essential metabolic processes. Third, Orn has additional moonlighting functions that are essential. Our findings rule out the third scenario, as diribonuclease activity, rather than the Orn protein itself, is required for cell viability. The essentiality of diribonuclease activity can be attributed to either the depletion of monoribonucleotides or the accumulation of diribonucleotides. Because the majority of RNA polymers (rRNA, tRNA, and mRNA) are degraded directly into monoribonucleotides (Figure 7) and growth on rich medium should, in addition, enable *de novo* synthesis of nucleotides, depletion of mononucleotides is an unlikely mechanism for the essentiality of diribonucleases. This leaves the intriguing possibility that accumulated diribonucleotides are biologically active molecules that negatively affect γ-proteobacteria. Data for RNase AM_{Pa} suggest that it has a stronger substrate preference but less activity than Orn (Figure S4), suggesting that only a subset of diribonucleotides is causing toxicity. Future work should identify the specific diribonucleotide(s) and the mechanisms that inhibit cell growth. A similar requirement for diribonucleases has been observed for NrnC[29] in α-proteobacteria, including *Caulobacter crescentus*, *Bartonella henselae*, and *Brucella abortus*,[40–42] suggesting that elevated diribonucleotides levels are detected in many organisms. The accumulation of diribonucleotides could serve as a signal to the cell that there is a defect in RNA degradation and recycling. One possibility is that these diribonucleotides act as nanoprimers.[43–45] Another possibility is that they interfere with other proteins in the cell. In *P. aeruginosa*, the ability of the Δ*orn* mutant to increase the expression of RNase AM_{Pa} suggests that this may serve as a quality control mechanism to reduce diribonucleotide levels. Since orthologs of *orn* are present in eukaryotes from yeast to plants to humans[46] and appear to be required for mitochondrial function,[47] this quality control mechanism for RNA degradation may be a broadly conserved process.

Limitations of the study

We show that in *P. aeruginosa*, there are two enzymes with diribonuclease activity, and we were able to verify their activity *in vivo* and *ex vivo* by generating mutants lacking one or the other gene. One major limitation is the inability to generate *orn* mutations in other γ-proteobacteria that also harbor both genes. The essentiality of *orn* in these organisms is well established and supports that Orn is the primary diribonuclease in those organisms. However, the contribution of RNase AM in those species could not be assessed independently of Orn. Future approaches to generate conditional mutations may reveal the functions of RNase AM.

RESOURCE AVAILABILITY

Lead contact

Further information and requests for resources and reagents should be directed to and will be fulfilled by the lead contact, Vincent T. Lee (vtlee@umd.edu).

Materials availability

All unique/stable reagents generated in this study are available from the lead contact with a completed materials transfer agreement.

Data and code availability

- Data are available in the manuscript and supplemental information. The structures were deposited in the PDB (PD: 9ETK).
- The mass spectrometry proteomics data have been deposited to the ProteomeXchange Consortium via the PRIDE partner repository with the dataset identifier PXD052373 and https://doi.org/10.6019/PXD052373.
- This paper does not report original code.
- Any additional information required to reanalyze the data reported in this paper is available from the lead contact upon request.

ACKNOWLEDGMENTS

We would like to thank the National Institutes of Health, United States for funding to V.T.L, H.S., and W.C.W. (R01 AI142400) and the National Research Foundation of Korea, South Korea for supporting S.-K.K. (2020R1C1C1004307).

AUTHOR CONTRIBUTIONS

Conceptualization, S.-K.K., H.S., W.C.W., and V.T.L.; investigation, S.-K.K., M.W.O., H.T., C.C.J., J.D.L., T.M.M., A.B., J.A.C., and W.C.K.; formal analyses, S.-K.K., M.W.O., H.T., C.C.J., J.D.L., T.M.M., A.B., and J.A.C.; data curation, S.-K.K., C.C.J., J.D.L., and A.B.; writing – original draft, S.-K.K., C.C.J., A.B., J.D.L., and V.T.L.; writing – review & editing, S.-K.K., M.W.O., H.T., C.C.J., T.M.M., A.B., J.A.C., X.J., H.S., W.C.W., and V.T.L.; visualization, J.D.L., H.S., A.B., and X.J.; funding acquisition, H.S., W.C.W., and V.T.L.

DECLARATION OF INTERESTS

The authors declare no competing interests.

STAR★METHODS

Detailed methods are provided in the online version of this paper and include the following:

- KEY RESOURCES TABLE
- EXPERIMENTAL MODEL AND STUDY PARTICIPANT DETAILS
  - Strains, plasmid, and growth condition
- METHOD DETAILS
  - Transposon mutagenesis screen
  - Sequencing of transposon mutants
  - Complementation with genomic fragments from transposon mutants
  - Preparation of whole cell lysates
  - Assay of enzyme activity
  - Site-directed mutagenesis
  - Labeling of RNAs

SUPPLEMENTAL INFORMATION

Supplemental information can be found online at https://doi.org/10.1016/j.celrep.2024.114759.

Received: May 15, 2024
Revised: July 29, 2024
Accepted: August 29, 2024
Published: September 13, 2024

REFERENCES

1. Jones, W. (1920). The action of boiled pancreas extract on yeast nucleic acid. Am. J. Physiol. *52*, 203–207.
2. Datta, A.K., and Niyogi, K. (1975). A novel oligoribonuclease of *Escherichia coli*. II. Mechanism of action. J. Biol. Chem. *250*, 7313–7319.
3. Niyogi, S.K., and Datta, A.K. (1975). A novel oligoribonuclease of *Escherichia coli*. I. Isolation and properties. J. Biol. Chem. *250*, 7307–7312.
4. Stevens, A., and Niyogi, S.K. (1967). Hydrolysis of oligoribonucleotides by an enzyme fraction from *Escherichia coli*. Biochem. Biophys. Res. Commun. *29*, 550–555.
5. Deutscher, M.P. (2006). Degradation of RNA in bacteria: comparison of mRNA and stable RNA. Nucleic Acids Res. *34*, 659–666. https://doi.org/10.1093/nar/gkj472.
6. Condon, C. (2007). Maturation and degradation of RNA in bacteria. Curr. Opin. Microbiol. *10*, 271–278. https://doi.org/10.1016/j.mib.2007.05.008.
7. Arraiano, C.M., Andrade, J.M., Domingues, S., Guinote, I.B., Malecki, M., Matos, R.G., Moreira, R.N., Pobre, V., Reis, F.P., Saramago, M., et al. (2010). The critical role of RNA processing and degradation in the control of gene expression. FEMS Microbiol. Rev. *34*, 883–923. https://doi.org/10.1111/j.1574-6976.2010.00242.x.
8. Hui, M.P., Foley, P.L., and Belasco, J.G. (2014). Messenger RNA degradation in bacterial cells. Annu. Rev. Genet. *48*, 537–559. https://doi.org/10.1146/annurev-genet-120213-092340.
9. Belasco, J.G. (2010). All things must pass: contrasts and commonalities in eukaryotic and bacterial mRNA decay. Nat. Rev. Mol. Cell Biol. *11*, 467–478. https://doi.org/10.1038/nrm2917.
10. Ghosh, S., and Deutscher, M.P. (1999). Oligoribonuclease is an essential component of the mRNA decay pathway. Proc. Natl. Acad. Sci. USA *96*, 4372–4377.
11. Ross, P., Weinhouse, H., Aloni, Y., Michaeli, D., Weinberger-Ohana, P., Mayer, R., Braun, S., de Vroom, E., van der Marel, G.A., van Boom, J.H., and Benziman, M. (1987). Regulation of cellulose synthesis in *Acetobacter xylinum* by cyclic diguanylic acid. Nature *325*, 279–281.
12. Chang, A.L., Tuckerman, J.R., Gonzalez, G., Mayer, R., Weinhouse, H., Volman, G., Amikam, D., Benziman, M., and Gilles-Gonzalez, M.A. (2001). Phosphodiesterase A1, a regulator of cellulose synthesis in *Acetobacter xylinum*, is a heme-based sensor. Biochemistry *40*, 3420–3426.
13. Cohen, D., Mechold, U., Nevenzal, H., Yarmiyhu, Y., Randall, T.E., Bay, D.C., Rich, J.D., Parsek, M.R., Kaever, V., Harrison, J.J., and Banin, E. (2015). Oligoribonuclease is a central feature of cyclic diguanylate signaling in *Pseudomonas aeruginosa*. Proc. Natl. Acad. Sci. USA *112*, 11359–11364. https://doi.org/10.1073/pnas.1421450112.
14. Orr, M.W., Donaldson, G.P., Severin, G.B., Wang, J., Sintim, H.O., Waters, C.M., and Lee, V.T. (2015). Oligoribonuclease is the primary degradative enzyme for pGpG in *Pseudomonas aeruginosa* that is required for cyclic-di-GMP turnover. Proc. Natl. Acad. Sci. USA *112*, E5048–E5057. https://doi.org/10.1073/pnas.1507245112.
15. Liberati, N.T., Urbach, J.M., Miyata, S., Lee, D.G., Drenkard, E., Wu, G., Villanueva, J., Wei, T., and Ausubel, F.M. (2006). An ordered, nonredundant library of *Pseudomonas aeruginosa* strain PA14 transposon insertion mutants. Proc. Natl. Acad. Sci. USA *103*, 2833–2838. https://doi.org/10.1073/pnas.0511100103.
16. Orr, M.W., Weiss, C.A., Severin, G.B., Turdiev, H., Kim, S.K., Turdiev, A., Liu, K., Tu, B.P., Waters, C.M., Winkler, W.C., and Lee, V.T. (2018). A subset of exoribonucleases serve as degradative enzymes for pGpG in c-di-GMP signaling. J. Bacteriol. *200*, e00300-18. https://doi.org/10.1128/JB.00300-18.
17. Kim, S.K., Lormand, J.D., Weiss, C.A., Eger, K.A., Turdiev, H., Turdiev, A., Winkler, W.C., Sondermann, H., and Lee, V.T. (2019). A dedicated diribonucleotidase resolves a key bottleneck for the terminal step of RNA degradation. Elife *8*, e46313. https://doi.org/10.7554/eLife.46313.
18. Kulasekara, H.D., Ventre, I., Kulasekara, B.R., Lazdunski, A., Filloux, A., and Lory, S. (2005). A novel two-component system controls the expression of *Pseudomonas aeruginosa* fimbrial *cup* genes. Mol. Microbiol. *55*, 368–380.
19. Ghodge, S.V., and Raushel, F.M. (2015). Discovery of a Previously Unrecognized Ribonuclease from *Escherichia coli* That Hydrolyzes 5'-Phosphorylated Fragments of RNA. Biochemistry *54*, 2911–2918. https://doi.org/10.1021/acs.biochem.5b00192.
20. Jean, J.M., and Hall, K.B. (2001). 2-Aminopurine fluorescence quenching and lifetimes: role of base stacking. Proc. Natl. Acad. Sci. USA *98*, 37–41. https://doi.org/10.1073/pnas.98.1.37.
21. Palace, S.G., Proulx, M.K., Lu, S., Baker, R.E., and Goguen, J.D. (2014). Genome-wide mutant fitness profiling identifies nutritional requirements for optimal growth of *Yersinia pestis* in deep tissue. mBio *5*, e01385-14. https://doi.org/10.1128/mBio.01385-14.
22. Kamp, H.D., Patimalla-Dipali, B., Lazinski, D.W., Wallace-Gadsden, F., and Camilli, A. (2013). Gene fitness landscapes of *Vibrio cholerae* at important stages of its life cycle. PLoS Pathog. *9*, e1003800. https://doi.org/10.1371/journal.ppat.1003800.
23. Sharma, S., Yang, J., Doamekpor, S.K., Grudizen-Nogalska, E., Tong, L., and Kiledjian, M. (2022). Identification of a novel deFADding activity in human, yeast and bacterial 5' to 3' exoribonucleases. Nucleic Acids Res. *50*, 8807–8817. https://doi.org/10.1093/nar/gkac617.
24. Cummings, J.A., Vetting, M., Ghodge, S.V., Xu, C., Hillerich, B., Seidel, R.D., Almo, S.C., and Raushel, F.M. (2014). Prospecting for unannotated enzymes: discovery of a 3',5'-nucleotide bisphosphate phosphatase within the amidohydrolase superfamily. Biochemistry *53*, 591–600. https://doi.org/10.1021/bi401640r.
25. van Kempen, M., Kim, S.S., Tumescheit, C., Mirdita, M., Lee, J., Gilchrist, C.L.M., Söding, J., and Steinegger, M. (2024). Fast and accurate protein structure search with Foldseek. Nat. Biotechnol. *42*, 243–246. https://doi.org/10.1038/s41587-023-01773-0.
26. Han, G.W., Ko, J., Farr, C.L., Deller, M.C., Xu, Q., Chiu, H.J., Miller, M.D., Sefcikova, J., Somarowthu, S., Beuning, P.J., et al. (2011). Crystal structure of a metal-dependent phosphoesterase (YP_910028.1) from *Bifidobacterium adolescentis*: Computational prediction and experimental validation of phosphoesterase activity. Proteins *79*, 2146–2160. https://doi.org/10.1002/prot.23035.
27. Corso, G., Deng, A., Fry, B., Polizzi, N., Barzilay, R., and Jaakkola, T. (2024). Deep Confident Steps to New Pockets: Strategies for Docking Generalization. Preprint at arXiv. https://doi.org/10.48550/arXiv.2402.18396.

28. Corso, G., Stärk, H., King, B., Barzilay, R., and Jaakkola, T. (2023). DiffDock: Diffusion Steps, Twists, and Turns for Molecular Docking.
29. Lormand, J.D., Kim, S.-K., Walters-Marrah, G.A., Brownfield, B.A., Fromme, J.C., Winkler, W.C., Goodson, J.R., Lee, V.T., and Sondermann, H. (2021). Structural characterization of NrnC identifies unifying features of dinucleotidases. Elife *10*, e70146. https://doi.org/10.7554/eLife.70146.
30. Jumper, J., Evans, R., Pritzel, A., Green, T., Figurnov, M., Ronneberger, O., Tunyasuvunakool, K., Bates, R., Žídek, A., Potapenko, A., et al. (2021). Highly accurate protein structure prediction with AlphaFold. Nature *596*, 583–589. https://doi.org/10.1038/s41586-021-03819-2.
31. Mirdita, M., Schütze, K., Moriwaki, Y., Heo, L., Ovchinnikov, S., and Steinegger, M. (2022). ColabFold: making protein folding accessible to all. Nat. Methods *19*, 679–682. https://doi.org/10.1038/s41592-022-01488-1.
32. Yu, D., Ellis, H.M., Lee, E.C., Jenkins, N.A., Copeland, N.G., and Court, D.L. (2000). An efficient recombination system for chromosome engineering in *Escherichia coli*. Proc. Natl. Acad. Sci. USA *97*, 5978–5983. https://doi.org/10.1073/pnas.100127597.
33. Murphy, K.C., Campellone, K.G., and Poteete, A.R. (2000). PCR-mediated gene replacement in Escherichia coli. Gene *246*, 321–330. https://doi.org/10.1016/s0378-1119(00)00071-8.
34. Datsenko, K.A., and Wanner, B.L. (2000). One-step inactivation of chromosomal genes in *Escherichia coli* K-12 using PCR products. Proc. Natl. Acad. Sci. USA *97*, 6640–6645. https://doi.org/10.1073/pnas.120163297.
35. Bremer, H., and Dennis, P.P. (2008). Modulation of Chemical Composition and Other Parameters of the Cell at Different Exponential Growth Rates. EcoSal Plus *3*. https://doi.org/10.1128/ecosal.5.2.3.
36. Zbornikova, E., Knejzlik, Z., Hauryliuk, V., Krasny, L., and Rejman, D. (2019). Analysis of nucleotide pools in bacteria using HPLC-MS in HILIC mode. Talanta *205*, 120161. https://doi.org/10.1016/j.talanta.2019.120161.
37. Varik, V., Oliveira, S.R.A., Hauryliuk, V., and Tenson, T. (2017). HPLC-based quantification of bacterial housekeeping nucleotides and alarmone messengers ppGpp and pppGpp. Sci. Rep. *7*, 11022. https://doi.org/10.1038/s41598-017-10988-6.
38. Jain, C. (2020). RNase AM, a 5' to 3' exonuclease, matures the 5' end of all three ribosomal RNAs in E. coli. Nucleic Acids Res. *48*, 5616–5623. https://doi.org/10.1093/nar/gkaa260.
39. Shatoff, E.A., Gemler, B.T., Bundschuh, R., and Fredrick, K. (2021). Maturation of 23S rRNA includes removal of helix H1 in many bacteria. RNA Biol. *18*, 856–865. https://doi.org/10.1080/15476286.2021.2000793.
40. Christen, B., Abeliuk, E., Collier, J.M., Kalogeraki, V.S., Passarelli, B., Coller, J.A., Fero, M.J., McAdams, H.H., and Shapiro, L. (2011). The essential genome of a bacterium. Mol. Syst. Biol. *7*, 528. https://doi.org/10.1038/msb.2011.58.
41. Liu, M.F., Cescau, S., Mechold, U., Wang, J., Cohen, D., Danchin, A., Boulouis, H.J., and Biville, F. (2012). Identification of a novel nanoRNase in *Bartonella*. Microbiology *158*, 886–895. https://doi.org/10.1099/mic.0.054619-0.
42. Sternon, J.F., Godessart, P., Goncalves de Freitas, R., Van der Henst, M., Poncin, K., Francis, N., Willemart, K., Christen, M., Christen, B., Letesson, J.J., and De Bolle, X. (2018). Transposon Sequencing of *Brucella abortus* Uncovers Essential Genes for Growth In Vitro and Inside Macrophages. Infect. Immun. *86*, e00312-18. https://doi.org/10.1128/IAI.00312-18.
43. Druzhinin, S.Y., Tran, N.T., Skalenko, K.S., Goldman, S.R., Knoblauch, J.G., Dove, S.L., and Nickels, B.E. (2015). A Conserved Pattern of Primer-Dependent Transcription Initiation in *Escherichia coli* and *Vibrio cholerae* Revealed by 5' RNA-seq. PLoS Genet. *11*, e1005348. https://doi.org/10.1371/journal.pgen.1005348.
44. Goldman, S.R., Sharp, J.S., Vvedenskaya, I.O., Livny, J., Dove, S.L., and Nickels, B.E. (2011). NanoRNAs prime transcription initiation in vivo. Mol. Cell *42*, 817–825. https://doi.org/10.1016/j.molcel.2011.06.005.
45. Skalenko, K.S., Li, L., Zhang, Y., Vvedenskaya, I.O., Winkelman, J.T., Cope, A.L., Taylor, D.M., Shah, P., Ebright, R.H., Kinney, J.B., et al. (2021). Promoter-sequence determinants and structural basis of primer-dependent transcription initiation in Escherichia coli. Proc. Natl. Acad. Sci. USA *118*, e2106388118. https://doi.org/10.1073/pnas.2106388118.
46. Zhang, X., Zhu, L., and Deutscher, M.P. (1998). Oligoribonuclease is encoded by a highly conserved gene in the 3'-5' exonuclease superfamily. J. Bacteriol. *180*, 2779–2781.
47. Bruni, F., Gramegna, P., Oliveira, J.M.A., Lightowlers, R.N., and Chrzanowska-Lightowlers, Z.M.A. (2013). REXO2 is an oligoribonuclease active in human mitochondria. PLoS One *8*, e64670. https://doi.org/10.1371/journal.pone.0064670.
48. Rahme, L.G., Stevens, E.J., Wolfort, S.F., Shao, J., Tompkins, R.G., and Ausubel, F.M. (1995). Common virulence factors for bacterial pathogenicity in plants and animals. Science *268*, 1899–1902.
49. Murphy, K.C. (1998). Use of bacteriophage lambda recombination functions to promote gene replacement in Escherichia coli. J. Bacteriol. *180*, 2063–2071. https://doi.org/10.1128/JB.180.8.2063-2071.1998.
50. Lee, V.T., Matewish, J.M., Kessler, J.L., Hyodo, M., Hayakawa, Y., and Lory, S. (2007). A cyclic-di-GMP receptor required for bacterial exopolysaccharide production. Mol. Microbiol. *65*, 1474–1484.
51. Furste, J.P., Pansegrau, W., Frank, R., Blocker, H., Scholz, P., Bagdasarian, M., and Lanka, E. (1986). Molecular cloning of the plasmid RP4 primase region in a multi-host-range tacP expression vector. Gene *48*, 119–131.
52. Kim, S.K., Lormand, J.D., Weiss, C.A., Eger, K.A., Turdiev, H., Turdiev, A., Winkler, W.C., Sondermann, H., and Lee, V.T. (2019). A dedicated diribonucleotidase resolves a key bottleneck for the terminal step of RNA degradation. Elife *8*, e46313. https://doi.org/10.7554/eLife.46313.
53. Schindelin, J., Arganda-Carreras, I., Frise, E., Kaynig, V., Longair, M., Pietzsch, T., Preibisch, S., Rueden, C., Saalfeld, S., Schmid, B., et al. (2012). Fiji: an open-source platform for biological-image analysis. Nat. Methods *9*, 676–682. https://doi.org/10.1038/nmeth.2019.
54. Kabsch, W. (2010). Xds. Acta Crystallogr. D Biol. Crystallogr. *66*, 125–132. https://doi.org/10.1107/S0907444909047337.
55. Liebschner, D., Afonine, P.V., Baker, M.L., Bunkóczi, G., Chen, V.B., Croll, T.I., Hintze, B., Hung, L.W., Jain, S., McCoy, A.J., et al. (2019). Macromolecular structure determination using X-rays, neutrons and electrons: recent developments in Phenix. Acta Crystallogr. D Struct. Biol. *75*, 861–877. https://doi.org/10.1107/S2059798319011471.
56. Seemann, T. (2014). Prokka: rapid prokaryotic genome annotation. Bioinformatics *30*, 2068–2069. https://doi.org/10.1093/bioinformatics/btu153.
57. Cantalapiedra, C.P., Hernández-Plaza, A., Letunic, I., Bork, P., and Huerta-Cepas, J. (2021). eggNOG-mapper v2: Functional Annotation, Orthology Assignments, and Domain Prediction at the Metagenomic Scale. Mol. Biol. Evol. *38*, 5825–5829. https://doi.org/10.1093/molbev/msab293.
58. Jones, P., Binns, D., Chang, H.Y., Fraser, M., Li, W., McAnulla, C., McWilliam, H., Maslen, J., Mitchell, A., Nuka, G., et al. (2014). InterProScan 5: genome-scale protein function classification. Bioinformatics *30*, 1236–1240. https://doi.org/10.1093/bioinformatics/btu031.
59. Huang, Y., Niu, B., Gao, Y., Fu, L., and Li, W. (2010). CD-HIT Suite: a web server for clustering and comparing biological sequences. Bioinformatics *26*, 680–682. https://doi.org/10.1093/bioinformatics/btq003.
60. Sievers, F., Wilm, A., Dineen, D., Gibson, T.J., Karplus, K., Li, W., Lopez, R., McWilliam, H., Remmert, M., Söding, J., et al. (2011). Fast, scalable generation of high-quality protein multiple sequence alignments using Clustal Omega. Mol. Syst. Biol. *7*, 539. https://doi.org/10.1038/msb.2011.75.
61. Minh, B.Q., Schmidt, H.A., Chernomor, O., Schrempf, D., Woodhams, M.D., von Haeseler, A., and Lanfear, R. (2020). IQ-TREE 2: New Models and Efficient Methods for Phylogenetic Inference in the Genomic Era. Mol. Biol. Evol. *37*, 1530–1534. https://doi.org/10.1093/molbev/msaa015.
62. Hoang, D.T., Chernomor, O., von Haeseler, A., Minh, B.Q., and Vinh, L.S. (2018). UFBoot2: Improving the Ultrafast Bootstrap Approximation. Mol. Biol. Evol. *35*, 518–522. https://doi.org/10.1093/molbev/msx281.

63. Kalyaanamoorthy, S., Minh, B.Q., Wong, T.K.F., von Haeseler, A., and Jermiin, L.S. (2017). ModelFinder: fast model selection for accurate phylogenetic estimates. Nat. Methods *14*, 587–589. https://doi.org/10.1038/nmeth.4285.

64. Letunic, I., and Bork, P. (2021). Interactive Tree Of Life (iTOL) v5: an online tool for phylogenetic tree display and annotation. Nucleic Acids Res. *49*, W293–W296. https://doi.org/10.1093/nar/gkab301.

65. Zhou, J., Opoku-Temeng, C., and Sintim, H.O. (2017). Fluorescent 2-Aminopurine c-di-GMP and GpG Analogs as PDE Probes. Methods Mol. Biol. *1657*, 245–261. https://doi.org/10.1007/978-1-4939-7240-1_19.

66. Myers, T.M., Ingle, S., Weiss, C.A., Sondermann, H., Lee, V.T., Bechhofer, D.H., and Winkler, W.C. (2023). *Bacillus subtilis* NrnB is expressed during sporulation and acts as a unique 3'-5' exonuclease. Nucleic Acids Res. *51*, 9804–9820. https://doi.org/10.1093/nar/gkad662.

67. Weiss, C.A., Myers, T.M., Wu, C.H., Jenkins, C., Sondermann, H., Lee, V.T., and Winkler, W.C. (2022). NrnA is a 5'-3' exonuclease that processes short RNA substrates in vivo and in vitro. Nucleic Acids Res. *50*, 12369–12388. https://doi.org/10.1093/nar/gkac1091.

68. Parks, D.H., Chuvochina, M., Rinke, C., Mussig, A.J., Chaumeil, P.A., and Hugenholtz, P. (2022). GTDB: an ongoing census of bacterial and archaeal diversity through a phylogenetically consistent, rank normalized and complete genome-based taxonomy. Nucleic Acids Res. *50*, D785–D794. https://doi.org/10.1093/nar/gkab776.

69. Emsley, P., Lohkamp, B., Scott, W.G., and Cowtan, K. (2010). Features and development of Coot. Acta Crystallogr. D Biol. Crystallogr. *66*, 486–501. https://doi.org/10.1107/S0907444910007493.

70. Yang, Y., Yu, Q., Wang, M., Zhao, R., Liu, H., Xun, L., and Xia, Y. (2022). Escherichia coli BW25113 Competent Cells Prepared Using a Simple Chemical Method Have Unmatched Transformation and Cloning Efficiencies. Front. Microbiol. *13*, 838698. https://doi.org/10.3389/fmicb.2022.838698.

STAR★METHODS

KEY RESOURCES TABLE

REAGENT or RESOURCE	SOURCE	IDENTIFIER
Bacterial and virus strains		
PA14	Rahme et al.[48]	N/A
PA14 pMMB	Orr et al.[16]	N/A
PA14 *Δorn*	Orr et al.[14]	N/A
PA14 *Δorn fleQ*::tn	This study	N/A
PA14 *Δorn yciI*::tn	This study	N/A
PA14 *Δorn yciB*::tn	This study	N/A
PA14 *Δorn PA14_22770*::tn	This study	N/A
PA14 *Δorn PA14_27420*::tn	This study	N/A
PA14 *Δorn ΔyciI*	This study	N/A
PA14 *Δorn ΔPA14_22770*	This study	N/A
PA14 *Δorn ΔcpxR*	This study	N/A
PA14 *Δorn* pMMB	Orr et al.[14]	N/A
PA14 *Δorn* pMMB *orn*	Orr et al.[14]	N/A
PA14 *Δorn* pMMB full fragment (FL)	This study	N/A
PA14 *Δorn* pMMB fragment 1 (F1)	This study	N/A
PA14 *Δorn* pMMB fragment 2 (F2)	This study	N/A
PA14 *Δorn* pMMB fragment 3 (F3)	This study	N/A
PA14 *Δorn* pMMB PA14 *yciV*	This study	N/A
PA14 *Δorn* pMMB $yciV_{Ec}$	This study	N/A
PA14 *Δorn* pMMB $yciV_{Vc}$	This study	N/A
PA14 *Δorn* pMMB $yciV_{St}$	This study	N/A
PA14 *Δorn* pMMB $yciV_{Yp}$	This study	N/A
PA14 *ΔyciV* pMMB	This study	N/A
PA14 *ΔyciV* pMMB *orn*	This study	N/A
PA14 *ΔyciV* pMMB F2	This study	N/A
E. coli BL21(DE3) pVL847 YciV	This study	N/A
E. coli BL21(DE3) pVL847 H38A	This study	N/A
E. coli BL21(DE3) pVL847 D39A	This study	N/A
E. coli BL21(DE3) pVL847 E63A	This study	N/A
E. coli BL21(DE3) pVL847 R101A	This study	N/A
E. coli BL21(DE3) pVL847 H194A	This study	N/A
E. coli BL21(DE3) pVL847 H253A	This study	N/A
E. coli BL21(DE3) pVL847 $YciV_{Ec}$	This study	N/A
E. coli BL21(DE3) pVL847 $YciV_{Vc}$	This study	N/A
E. coli BL21(DE3) pVL847 $YciV_{St}$	This study	N/A
E. coli BL21(DE3) pVL847 $YciV_{Yp}$	This study	N/A
E. coli TW6	Murphy et al.[49]	N/A
E. coli TW6 pMMB	This study	N/A
E. coli TW6 pMMB *orn*	This study	N/A
E. coli TW6 pMMB *orn* H158A	This study	N/A
E. coli TW6 pMMB F2	This study	N/A
E. coli TW6 pMMB *yciV* R101A	This study	N/A

(*Continued on next page*)

Continued

REAGENT or RESOURCE	SOURCE	IDENTIFIER
Chemicals, peptides, and recombinant proteins		
Lysogeny broth (LB)	RPI	Cat# L24060
Gentamicin	Goldbio	Cat# G400
Carbenicillin	Goldbio	Cat# C0109
Chloramphenicol	RPI	Cat# C61000
Sucrose	RPI	Cat# S24060
Irgasan	Sigma	Cat# 72779
Kanamycin	Goldbio	Cat# K120
Calf intestinal phosphatase (CIP)	New England Biolabs	Cat# M0290
Isopropyl-β-D-1-thiogalactopyranoside (IPTG)	Goldbio	Cat# I2481C50
NaCl	Fisher	Cat# S640-10
Tris	RPI	Cat# T60040
Lysozyme	Roche	Cat# 837059
DNase	Roche	Cat# 104159
Phenylmethylsulfonyl fluoride (PMSF)	Goldbio	Cat# P-470-10
Urea	RPI	Cat# U20200
Manganese(II) chloride	Sigma	Cat# 244589
Magnesium chloride hexahydrate	Fisher	Cat# M33
Ethylenediaminetetraacetic acid (EDTA)	RPI	Cat# E57020
T4 polynucleotide kinase	New England Biolabs	Cat# M0201S
2-aminopurine	GE Healthcare Dharmacon	–
Imidazole	Fisher	Cat# AC122020020
Acetonitrile	Sigma	Cat# 34851
Dithiothreitol (DTT)	RPI	Cat# D11000
Methanol	Sigma	Cat# 34860
Trypsin/Lys-C	Promega	Cat# V5071
Sodium dodecyl sulfate (SDS)	RPI	Cat# L22040
Tetraethylammonium bromide (TEAB)	Sigma	Cat# 140023
Formic acid	Sigma	Cat# F0507
Glycerol	Fisher	Cat# G33
HEPES	RPI	Cat# H75030
Bis-Tris	RPI	Cat# B78000
Ammonium sulfate	Fisher	Cat# A649
Polyethylene glycerol 8000 (PEG 8000)	RPI	Cat# P48080
Dimethyl sulfoxide (DMSO)	Fisher	Cat# 036480.AP
pApA*ps*Gp(2AP)	GE Healthcare Dharmacon	–
p(2AP)pA*ps*GpG	GE Healthcare Dharmacon	–
DpnI	New England Biolabs	Cat# R0176S
Wizard Plus SV miniprep DNA purification Kit	Promega	Cat# A1465
Wizard gDNA preparation Kit	Promega	Cat# A1125
Q5 Site-Directed Mutagenesis Kit	New England Biolabs	Cat# E0552S
Pierce™BCA Protein Assay kit	Thermo Fisher Scientific	Cat# 23227
StuI	New England Biolabs	Cat# R0187S
AluI	New England Biolabs	Cat# R0137S
Ni-NTA resin	Thermo Fisher Scientific	Cat# PI88222
Ulp-1 protease	Thermo Fisher Scientific	Cat# 12588018
Oligonucleotides		
Primer sequence used for vector construction	–	This study
5′-GG-3′	Sigma	–

(*Continued on next page*)

Continued

REAGENT or RESOURCE	SOURCE	IDENTIFIER
5′-AAAAAGG-3′	Sigma	–
Recombinant DNA		
pBT20	Kulasekara et al.[18]	N/A
pSMN10 - *ΔyciV*	This study	N/A
pSMN10 - *ΔyciI*	This study	N/A
pSMN10 - *ΔPA14_22770*	This study	N/A
pSMN10 - *ΔcpxR*	This study	N/A
pVL847	Lee et al.[50]	N/A
pET28a	Novagen	–
pVL847 PA14 *yciV*	This study	N/A
pVL847 H38A	This study	N/A
pVL847 D39A	This study	N/A
pVL847 E63A	This study	N/A
pVL847 R101A	This study	N/A
pVL847 H194A	This study	N/A
pVL847 H253A	This study	N/A
pVL847 *E coli yciV*	This study	N/A
pVL847 *V cholerae yciV*	This study	N/A
pVL847 *S enterica yciV*	This study	N/A
pVL847 *Y. pseudotubelculosis yciV*	This study	N/A
pMMB	Fürste et al.[51]	N/A
pMMB full fragment (FL)	This study	N/A
pMMB fragment 1 (F1)	This study	N/A
pMMB fragment 2 (F2)	This study	N/A
pMMB fragment 3 (F3)	This study	N/A
pMMB PA14 *yciV*	This study	N/A
pMMB H38A	This study	N/A
pMMB D39A	This study	N/A
pMMB E63A	This study	N/A
pMMB R101A	This study	N/A
pMMB H194A	This study	N/A
pMMB H253A	This study	N/A
pMMB *E. coli yciV*	This study	N/A
pMMB *V. cholerae yciV*	This study	N/A
pMMB *S. enterica yciV*	This study	N/A
pMMB *Y. pseudotubelculosis yciV*	This study	N/A
pMMB *orn*	This study	N/A
pMMB *orn* H158A	Kim et al.[52]	N/A
pKD3	Datsenko and Wanner[34]	N/A
Software and algorithms		
Fiji (Fiji is just ImageJ),	Schindelin et al.[53]	https://imagej.net/software/fiji/
GraphPad Prism	GraphPad	https://www.graphpad.com/
Multi Gauge software v3.0	Fujifilm	N/A
Proteome Discoverer ver. 2.5.0.400	Thermo Fisher Scientific	https://www.ncbi.nlm.nih.gov/pmc/articles/PMC8006021
XDS	Kabsch[54]	–
Phenix	Liebschner et al.[55]	–
AlphaFold2	Jumper et al.[30]	https://alphafold.ebi.ac.uk/
ColabFold	Mirdita et al.[31]	https://colabfold.mmseqs.com/

(*Continued on next page*)

Continued

REAGENT or RESOURCE	SOURCE	IDENTIFIER
PyMOL Molecular Graphics System, Version 1.2r3pre	Schrödinger, Inc	https://raw.githubusercontent.com/Pymol-Scripts/Pymol-script
Prokka, version 1.14.6	Seemann[56]	–
eggNOG-mapper version 2.1.3	Cantalapiedra et al.[57]	–
InterProScan 5 (version 5.60–92.0)	Jones et al.[58]	–
CD-HIT (version 4.8.1)	Huang et al.[59]	–
Clustal Omega, version 1.2.4	Sievers et al.[60]	–
IQ-TREE, version 2.1.2	Minh et al.[61]	http://www.iqtree.org
UFBoot2	Hoang et al.[62]	–
ModelFinder	Kalyaanamoorthy et al.[63]	–
iTOL	Letunic and Bork[64]	–
DiffDock-L	Corso et al.[27,28]	https://huggingface.co/spaces/reginabarzilaygroup/DiffDock-Web

EXPERIMENTAL MODEL AND STUDY PARTICIPANT DETAILS

Strains, plasmid, and growth condition

Stains and plasmids used are listed in key resources table. *P. aeruginosa* and *E. coli* were grown in lysogeny broth (LB) at 37°C. Plasmid are maintained using antibiotics at 15 μg/mL gentamicin, 50 μg/mL carbenicillin, and 10 μg/mL chloramphenicol, where appropriate. In-frame deletion mutants of *P. aeruginosa* were generated by conjugation of a non-replicative plasmid containing 1 kilobase upstream and downstream of the gene to be deleted. *P. aeruginosa* co-integrants were selected using 75 μg/mL gentamicin and 25 μg/mL irgasan. The plasmid was counter-selected by plating on 6% sucrose. In-frame deletion mutants were screened by PCR.

METHOD DETAILS

Transposon mutagenesis screen

The pBT20 mariner transposon from *E. coli* SM10 λpir was introduced into *P. aeruginosa* PA14 *Δorn* by conjugation.[18] The bacteria were mixed and 50 μL were spotted onto a pre-dried and prewarmed LB agar plate. The spots were allowed to fully absorb and dry for ~10 min and incubated for an additional 90 min at 37°C. Each spot was swabbed and resuspended in 1 mL LB. Two hundred microliters of each resuspension were plated onto an LB agar plate containing 75 μg/mL gentamicin and 25 μg/mL irgasan, yielding ~100–150 colonies per plate. A total of 250 plates were generated, yielding ~40,000 colonies. After overnight incubation at 37°C, colonies were visually screened for increased colony size. Colonies of interest were picked, restruck for single colonies for validation of colony size changes, and saved for sequencing.

Sequencing of transposon mutants

Genomic DNA was isolated using ArchivePure DNA Cell/Tissue Kit (5 PRIME) according to manufacturer's instructions. Purified genomic DNA was digested using the blunt cutting restriction enzymes StuI and MscI according to manufacturer's instructions (New England Biolabs). The digested genomic DNA was cloned into StuI linearized pCR-blunt and plated on an LB agar plate containing 50 μg/mL kanamycin and 15 μg/mL gentamicin. Resulting colonies were isolated and miniprepped using Wizard Plus SV Miniprep DNA Purification Kit (Promega) and sequenced using the transposon specific (and/or plasmid specific) primers.

Complementation with genomic fragments from transposon mutants

The *P. aeruginosa* PA14 *Δorn*, PA14 *Δorn ycil::tn,* PA14 *Δorn fleQ::tn,* and PA14 *Δorn PA14_27420::tn* strains were grown on LB agar plate containing 15 μg/mL gentamicin, then inoculated into LB supplemented with 15 μg/mL gentamicin at 37°C with shaking overnight. Genomic DNA was extracted from cultures using Wizard gDNA preparation kit (Promega). Extracted gDNA was digested for 1 h using serial diluted amounts of AluI to generate blunt fragments. The digested DNA was separated on 1% TAE agarose gel. DNA fragments with sizes between ~4 and 9 kb were gel purified, and cloned into pMMB vector that was digested with SmaI and treated with calf intestinal phosphatase (CIP). This yielded ~20,000 colonies. The collected transformants were subsequently mated with PA14 *P. aeruginosa Δorn* strain and plated on LB supplemented with 25 μg/mL irgasan and 150 μg/mL carbenicillin resulting in ~100,000 colonies. Colonies with increased colony size were retested in liquid culture (LB with 50 μg/mL carbenicillin) to identify cells that grew similar to the parental PA14 strain. Plasmids from suppressor strains were miniprepped and sequence to determine the genomic fragments responsible for suppression the Δ*orn* mutation.

Preparation of whole cell lysates

Overnight cultures of *P. aeruginosa* PA14 *Δorn*, or complemented strains were subcultured into fresh media with 50 μg/mL carbenicillin and 1 mM IPTG, grown at 37°C with shaking. All bacteria samples were collected by centrifuge and resuspended in 1/10 volume of 100 mM NaCl, and 10 mM Tris, pH 8, also supplemented with 25 μg/mL lysozyme, 10 μg/mL DNase, and 1mM PMSF and stored at −80°C.

Assay of enzyme activity

The activity of whole cell lysates against ^{32}P-labeled substrates was measured by the appearance of ^{32}P-labeled substrates on 20% Urea PAGE containing 1× TBE buffer. The reactions including phosphorylated RNA (1 μM) and trace amount of radiolabeled substrate were performed at room temperature in reaction buffer (10 mM Tris, pH 8, 100 mM NaCl, 5 mM $MgCl_2$ and 10 μM $MnCl_2$). At indicated time, the reaction was stopped by transferring 2 μL of the reaction to tubes containing 5 μL of 0.2 M EDTA and heated at 98°C for 5 min. Samples were separated on 20% urea PAGE containing 1× TBE buffer and 4 M urea. The gel was exposure to phosphorimager screen and imaged using Fujifilm FLA-7000 phosphorimager (GE). The intensity of the radiolabeled nucleotides was quantified using Fujifilm Multi Gauge software v3.0.

Site-directed mutagenesis

yciV site-directed mutagenesis were generated by using primers in Table S1 with the Q5 Site-Directed Mutagenesis Kit (New England Biolabs).

Labeling of RNAs

5′ unphosphorylated RNAs were purchased from TriLink Biotechnologies or Sigma. The single-strand oligoribonucleotides (GG or AAAAAGG) were used for 5′-labeled ^{32}P with T4 polynucleotide kinase (New England Biolabs) and [γ-^{32}P]-ATP. Reactions were incubated at 37°C for 1 h followed by heat inactivation of T4 PNK at 90°C for 10 min.

Aggregation assay

Indicated strain of *P. aeruginosa* are grown in LB agar plates supplemented with 15 μg/mL gentamicin. Three independent colonies were inoculated into glass tubes containing 2.5 mL of LB supplemented with 10 μg/mL gentamicin. The cultures were incubated in a fly-wheel in 37°C for 16 h. Culture tubes were photographed.

Colony morphology

Strains were grown overnight in LB media supplemented with 50 μg/mL carbenicillin. Strains were normalized to OD_{600} 0.5, serial diluted to achieve 5 CFU/μL, then 10 μL were dripped in parallel on LB agar plate containing 50 μg/mL carbenicillin and 1 mM IPTG. Strains were grown at 37°C for 30 h then imaged. Colonies sizes were measured by Fiji. For all strains, the control strains were always included on the same plate.

2-Aminopurine RNase assays

To investigate the rate of diribonucleotide processing and to determine the polarity of RNase AM protein homologs, we utilized an assay based on the differential fluorescence output of the nucleotide analog 2-aminopurine (2-AP) as described previously.[65–67] This assay exploits the different fluorescent properties of 2-AP as this nucleobase exhibits reduced fluorescence output when base stacked with other nucleobases but shows an increase in fluorescence output when liberated from an RNA polymer by a phosphodiesterase cleavage event. The RNA substrate pAp(2AP) and the tetraribonucleotide substrates containing internal, potentially non-hydrolyzable phosphorothioate (*ps*) linkages pAp*A*p*s*Gp(2AP) and p(2AP)p*A*p*s*GpG were all purchased as purified HPLC purified single stranded RNAs from GE Healthcare Dharmacon. These reactions were conducted at room temperature in a volume of 75 μL in a black Corning 384 well plate in the presence of 10 mM Tris-HCl, pH 8.0, 100 mM NaCl, 5 mM $MgCl_2$, 10 μM $MnCl_2$ 5 μM of the indicated 2-AP containing RNA substrate, and the respective protein concentration. 2-AP release was monitored using a Spectramax M5 plate reader with the excitation wavelength set to 310 nm and the emission wavelength at 375 nm.

Sample preparation for proteomic analysis

All reagents utilized during the proteomic sample preparation and analysis were mass spectrometry grade. Cells were harvested by centrifugation followed by sonication in 100 μL of 20% SDS, 100 mM TEAB. Protein quantification was performed by Pierce BCA Protein Assay Kit (PN: 23227) according to the manufacturers protocol. Samples were normalized to 300 μg/100μL protein concentration. Further sample preparation was performed according to the Protifi S-Trap mini protocol adjusted for a 100 μL starting sample. Briefly, samples were reduced by addition of DTT to 20 mM final concentration at 95°C for 10 min, followed by alkylation via addition of iodoacetamide to a final concentration of 0.1 M for 30 min, followed by acidification via formic acid to 1.5% final concentration. Finally, samples were mixed with 6X volume S-Trap buffer (90% methanol with 100 mM TEAB) and loaded into S-Trap Mini columns. Trypsin/Lys-C (Promega, Madison WI, U.S.A.) was added at a 1:20 trypsin:protein ratio. Samples were then dried to completion in a cold-trap vacuum centrifuge.

Mass spectrometry analysis

Proteomics samples were resuspended to 0.5 μg/μL and analyzed on a Thermo Eclipse mass spectrometer with FAIMS interface, coupled to an UltiMate 3000 HPLC (Thermo Fisher Scientific). 6 μL of sample was trapped on a PepMap 100, 75 μm id × 2 cm C18 trap column (Thermo Fisher Scientific) at 3 μL/min for 10 min with 2% acetonitrile (v/v) and 0.05% formic acid (v/v). Chromatographic separation was performed by an Easy-Spray 75 μm id × 75 cm length, 2 μm, 100 Å C18 column (Thermo Fisher Scientific) at 55°C. Samples were resolved using a 200 min gradient that with the following elution parameters utilizing mobile phases A (0.1% formic acid in water) and B (80% acetonitrile +0.1% formic acid in water) at a flow rate of 300 nL/min: 5% B:0 min, 10% B:5 min, 90% B:161 min, 90% B:171 min, 5% B: 181 min. The Thermo Eclipse was operated in positive polarity and data dependent mode (top-12, 3 s cycle time) with a dynamic exclusion of 60 s (with 5 ppm error). FAIMS CVs were set to −50 V, −65 V, and −85 V, with the 3 s cycle time split between each CV. MS1 scan resolution using the Orbitrap was set at 240,000 and the mass range was set to 350 to 2000 m/z. Normalized AGC target was set to 250%, with maximum injection time set to auto. Monoisotopic peak determination was used, specifying peptides and intensity threshold of 5 x 10^3 was used for precursor selection. Data-dependent MS2 fragmentation was performed using higher-energy collisional dissociation (HCD) at a collision energy of 28% with quadrupole isolation at 1 m/z width. Ion trap scan rate was set to turbo, with a maximum injection time of 35 ms.

Proteomic data analysis

Proteomic data analysis was performed utilizing Proteome Discoverer ver. 2.5.0.400. Database searching was performed by Sequest HT against the PA14 strain proteome downloaded from the Pseudomonas Genome DB (05/03/2023). Precursor and fragment mass tolerances were set at 10 ppm and 0.6 Da respectively. Peptide modification include in the search were are follows; dynamic modifications: Oxidation on M, Deamidation on N, Q, and R, dynamic protein N terminus modifications: Acetyl, Met-loss, and Met-loss+Acetylation, and static modifications: carbamidomethylation on C. False discovery rate for peptide identification was performed utilizing Percolator with strict and relaxed cutoffs set to 0.01 and 0.05 respectively. Feature detection for label free quantification was performed with the Minora Feature detection node requiring high PSM confidence for feature mapping. Feature mapping was set to a align features within a 10 ppm tolerance and 10 min maximum retention time shift. Feature normalization was performed on total peptide amount and quantification was performed utilizing a top 3 summed abundance strategy. Abundance comparison and significance calculation was performed by pairwise ratios and t test respectively. Post hoc significance analysis was performed with the Benjamini-Hochberg method.

Phylogenetic analysis

All representative genomes from Genome Taxonomy Database (GTDB)(release r207)[68] were downloaded and protein sequences for each genome were predicted using prokka (version 1.14.6).[56] Proteins predicted to belong to COG0613 by eggnog-mapper (version 2.1.3)[57] and SSF89550 based on interproscan(version 5.60–92.0)[58] were retrieved. These sequences were clustered to 70% identity with CD-HIT (version 4.8.1) to remove redundancy.[59] The dataset was filtered to remove sequences below 200 amino acids and above 400 amino acids. RNase AM sequences of interest were added into the dataset to assure their inclusion with NCBI gene identifiers ABJ12426.1 (*Pseudomonas aeruginosa*), NP_460680.1 (*Salmonella typhimurium*), NP_230822.1 (*Vibrio cholerae*), NP_415782.1 (*Escherichia coli*), YP_002347182.1 (*Yersinia pestis*) and WP_011135245.1 (*Chromobacterium violaceum*). The remaining 1,621 sequences were aligned with Clustal Omega (version 1.2.4) and default options.[60] A phylogenetic tree of the *yciV* genes was inferred with IQ-TREE (version 2.1.2)[61] with 10,000 ultrafast bootstrap replicates (UFBoot)[62] using ModelFinder to determine the best model of evolution.[63] Trees were visualized in iTOL.[64]

Cloning, protein expression and purification

The open reading frame of RNase AM_{Vc} (VC1177) from *Vibrio cholerae* O1 El Tor (residues 1–290) was codon optimized for expression in *E. coli* and synthesized by GeneArt (Life Technologies). The DNA fragment was inserted by In-Fusion seamless cloning (Takara) between BamHI and NotI sites of a modified pET28a vector (Novagen) yielding N-terminally His6-tagged small ubiquitin-like modifier (SUMO) fusion proteins cleavable by recombinant Ulp-1 protease. Plasmids were verified by Sanger sequencing (Microsynth AG).

RNase AM_{Vc} was overexpressed in *E. coli* BL21 T7 Express cells (New England Biolabs) from fresh transformants. Protein expression was induced with 0.5 mM IPTG for 16 h at 16°C after reaching an OD_{600} = 1.0 in Terrific broth (TB) supplemented with 50 μg/mL kanamycin initially grown at 37°C in a shaking incubator. Cells were harvested by centrifugation, resuspended in a minimal volume of Ni-NTA binding buffer (25 mM Tris-Cl pH 8.5, 500 mM NaCl, 20 mM imidazole, 10% glycerol) and flash frozen in liquid nitrogen. After thawing, cells were lysed on ice by sonication, and insoluble debris was pelleted by centrifugation for 45 min at 40,000g and 4°C. All further purification steps were carried out at 4°C. Soluble supernatant was incubated with Ni-NTA resin (Qiagen) pre-equilibrated with Ni-NTA binding buffer for 1 h on ice with gentle agitation. RNase AM_{Vc}-bound resin was washed with three rounds of 10 column volumes (CV) Ni-NTA binding buffer by gravity flow, followed by elution with three rounds of 2 CV Ni-NTA elution buffer (25 mM Tris-HCl pH 8.5, 500 mM NaCl, 400 mM imidazole, 10% glycerol). Eluates were buffer exchanged into gel filtration buffer (25 mM HEPES-NaOH pH 7.5, 500 mM NaCl, 10% glycerol) with a HiPrep 26/10 desalting column (Cytiva) followed by overnight cleavage of the His_6-SUMO moiety by Ulp1-His_6. RNase AM_{Vc} was separated from His-tagged Ulp-1 and SUMO by flowing-through a HisTrap Ni-NTA column (Cytiva). EDTA was added to the flow through containing RNase AM_{Vc} at a final concentration of 10 mM, followed

by concentration of RNase AM_{Vc} with an Amicon Ultra 10K concentrator (Merck Millipore). Concentrated RNase AM_{Vc} was injected onto a HiLoad 16/600 Superdex 200 gel filtration column (Cytiva) equilibrated in gel filtration buffer, and pure RNase AM_{Vc} fractions were pooled, concentrated to >30 mg/mL, frozen in liquid nitrogen and stored at −80°C.

Crystallization, data collection, and structure refinement

RNase AM_{Vc} crystals were prepared in gel filtration buffer in the presence of pGpG (Jena BioScience) by mixing RNase AM:pGpG in a 1:2 ratio followed by incubation at 19°C for 30 min. Protein concentrations used in crystallization ranged from 5 to 20 mg/mL. Crystals were grown by hanging-drop vapor diffusion by mixing equal volumes (0.8 μL) of sample with reservoir solution. RNase AM_{Vc} crystals grew at 19°C over a reservoir solution of 0.1 M Bis-Tris (pH 5.0), 0.2 M ammonium sulfate and 22.5% PEG 3350. Crystals were soaked in cryo-protectant composed of reservoir solution supplemented with 25% glycerol and frozen in liquid nitrogen. Data were collected by synchrotron radiation on frozen crystals at beamline P11 at Deutsches Elektronen-Synchrotron DESY, Hamburg, Germany. Diffraction datasets were processed using XDS,[54] and initial structures were solved by molecular replacement using the software package Phenix[55] with the coordinates of CV1693 (PDB: 2yb1[24]) as the search model. Manual model building and refinement were carried out with Coot[69] and Phenix. Illustrations were prepared in Pymol (The PyMOL Molecular Graphics System, Version 3.0 Schrödinger, Inc). All data collection and refinement statistics are summarized in Figure S5.

Data deposition

The atomic coordinates and structure factors have been deposited in the Protein DataBank, www.rcsb.org (PDB ID 9ETK).

Computational structural biology approaches

We used AlphaFold2 and ColabFold to predict the structure of monomeric RNase AM_{Pa} using default parameters.[30,31] Five models were generated and ranked. The top-ranked model was relaxed by molecular dynamics within ColabFold. To dock pGpG to the crystal structure of RNase AM_{Vc}, we employed the DiffDock-L method using the DiffDock web interface (https://huggingface.co/spaces/reginabarzilaygroup/DiffDock-Web).[27,28] The crystallographic model of the protein from the final refinement step and the SMILES string for pGpG were used as the inputs. Structural homology searches were carried out using Foldseek with the crystal structure of RNase AM_{Vc} as input and the PDB100 database as the search space.[25] Structures were visualized in PyMOL, and rmsd values were calculated and illustrated using the PyMOL script ColorByRMSD and a custom color gradient (https://raw.githubusercontent.com/Pymol-Scripts/Pymol-scriptrepo/master/colorbyrmsd.py) (The PyMOL Molecular Graphics System, Version 1.2r3pre, Schrödinger, LLC.).

orn gene disruption in *E. coli*

PCR products were generated using *E. coli* K12 Δ*orn* forward and *E. coli* K12 Δ*orn* reverse primers (Table S1), which included homology extensions for *orn* from *E. coli* and priming sequences for pKD3[34] as a template. PCR products were then purified and treated with DpnI. *E. coli* TW6 was cultured in 20 mL LB containing 15 μg/mL gentamicin and 1 mM IPTG and grown to OD_{600} 0.5 at 30°C, followed by a heat shock at 42°C for 15 min. Cells were collected by centrifugation at 3,220 *g* for 10 min and washed 2 times with ice-cold TSS buffer (10% PEG8000, 5% DMSO, 10% glycerol, 10 mM $MgSO_4$, 10 mM $MgCl_2$).[70] PCR products were transformed into *E. coli* TW6 with pMMB, or pMMB-*orn*, or pMMB-F2 by incubation on ice for 30 min, heat shock for 42°C for 30 s, followed incubation on ice for 2 min. Cells were recovered by addition of 100 μL of LB and incubated 1 h at 30°C with shaking. Cells were spread onto LB agar with 10 μg/mL chloramphenicol, 15 μg/mL gentamicin and 1 mM IPTG for 48 h at 30°C.

QUANTIFICATION AND STATISTICAL ANALYSIS

All data were performed two times or more independent under condition. Statical analyses were performed using Prism 7 software.